https://doi.org/10.5194/cp-2020-108
Preprint. Discussion started: 4 September 2020

Climate of the Past Discussions

Climate, cryosphere and carbon cycle controls on Southeast Atlantic orbital-scale carbonate deposition since the Oligocene (30-0 Ma)

Anna Joy Drury[1,2*], Diederik Liebrand[1], Thomas Westerhold[1], Helen M. Beddow[3], David A. Hodell[4], Nina Rohlfs[1], Roy H. Wilkens[5], Mitch Lyle[6], David B. Bell[7], Dick Kroon[7], Heiko Pälike[1], Lucas J. Lourens[3]

[1]MARUM-Center for Marine Environmental Sciences, University of Bremen, Leobener Strasse 8, 28359 Bremen, Germany
[2]Department of Earth Sciences, University College London, Gower Street, London, WC1E 6BT, UK.
[3]Department of Earth Sciences, Faculty of Geosciences, Utrecht University, Utrecht, The Netherlands
[4]Department of Earth Science, University of Cambridge, Cambridge, UK
[5]University of Hawaii, School of Ocean and Earth Science and Technology, Honolulu, Hawaii 96822, USA
[6]College of Earth, Ocean, and Atmospheric Science, Oregon State University, Corvallis, Oregon 97331, USA
[7]School of GeoSciences, University of Edinburgh, Edinburgh, UK

Correspondence to: ajdrury@marum.de; a.j.drury@ucl.ac.uk

Abstract The evolution of the Cenozoic Icehouse over the past 30 million years (Myr) from a unipolar to a bipolar world is broadly known; however, the exact development of orbital-scale climate variability is less well understood. Highly resolved records of carbonate ($CaCO_3$) content provide insight into the evolution of regional and global climate, cryosphere and carbon cycle dynamics. Here, we generate the first Southeast Atlantic $CaCO_3$ content record spanning the last 30 Myr, derived from X-ray fluorescence (XRF) ln(Ca/Fe) data collected at Ocean Drilling Program Site 1264 (Angola Basin side of the Walvis Ridge, SE Atlantic Ocean). We present a comprehensive and continuous depth and age model for the entirety of Site 1264 (~316 m; 30 Myr), which constitutes a key reference framework for future palaeoclimatic and palaeoceanographic studies at this site. We identify three phases with distinctly different orbital controls on Southeast Atlantic $CaCO_3$ deposition, corresponding to major developments in climate, the cryosphere and/or the carbon cycle: 1) strong ~110 kyr eccentricity pacing prevails during Oligo-Miocene global warmth (~30-13 Ma); 2) increased eccentricity-modulated precession pacing appears after the mid Miocene Climate Transition (mMCT) (~14-8 Ma); 3) strong obliquity pacing appears in the late Miocene (~7.7-3.3 Ma) following the increasing influence of high-latitude processes. The lowest $CaCO_3$ content (92-94%) occur between 18.5-14.5 Ma, potentially reflecting dissolution caused by widespread early Miocene warmth and preceding Antarctic deglaciation across the Miocene Climate Optimum (~17-14.5 Ma) by 1.5 Myr. The emergence of precession-pacing of $CaCO_3$ deposition at Site 1264 after ~14 Ma could signal a reorganisation of surface and/or deep-water circulation in this region following Antarctic reglaciation at the mMCT. The increased sensitivity to precession at Site 1264 is associated with an increase in mass accumulation rates (MARs) and reflects increased regional $CaCO_3$ productivity and/or an influx of cooler, less corrosive deep-waters. The highest %$CaCO_3$ and MARs indicate the late Miocene Biogenic Bloom (LMBB) occurs between ~7.8-3.3 Ma at Site 1264, which is broadly, but not exactly, contemporaneous with the LMBB in the equatorial Pacific Ocean. The global expression of the LMBB may reflect an increased nutrient input into the global ocean resulting from enhanced aeolian dust and/or glacial/chemical weathering fluxes. Regional variability in the timing and amplitude of the LMBB may be driven by regional differences in cooling, continental aridification and/or changes in ocean circulation in the late Miocene.

https://doi.org/10.5194/cp-2020-108
Preprint. Discussion started: 4 September 2020

Climate of the Past Discussions

1 Introduction

Over the last 30 Million years (Myr), Earth's climate system evolved considerably from the early unipolar Antarctic icehouse to our modern-day bipolar world (Zachos et al., 2001; De Vleeschouwer et al., 2017; Littler et al., 2019). Inferred from benthic foraminiferal oxygen isotope data ($\delta^{18}O$), the Oligocene-early Miocene (30-17 million years ago [Ma]) was characterized by variable Antarctic ice sheets. This Unipolar icehouse was marked by high amplitude glacial-interglacial cycles that were predominantly eccentricity paced (Wade, 2004; Pälike et al., 2006; Liebrand et al., 2016, 2017; Beddow et al., 2018). During the warm Miocene Climatic Optimum (MCO; 17-14.7 Ma), the Antarctic ice sheet shrank relative to its early Miocene size (Shevenell et al., 2004, 2008; Holbourn et al., 2015; Gasson et al., 2016; Levy et al., 2016), before prevalent unipolar icehouse conditions were re-established when Antarctica reglaciated across the mid Miocene Climate Transition (mMCT) around ~13.9 Ma (Shevenell et al., 2004, 2008; Holbourn et al., 2005, 2014; Levy et al., 2016). Following the onset of strong obliquity pacing at ~7.7 Ma (Drury et al., 2017, 2018b) and further global cooling during the late Miocene-early Pliocene (7-5 Ma, Herbert et al., 2016), a fully bipolar Icehouse world was established at ~2.7 Ma (Bailey et al., 2013).

The evolution of orbital-scale climate and carbon cycle dynamics across this interval remains relatively unscrutinised (Turner, 2014; De Vleeschouwer et al., 2017). High-resolution carbonate records provide insight into past dynamics and long-term evolution of the carbon cycle. Carbonate deposition is largely controlled by a combination of the amount of biogenic carbonate productivity in the surface waters and the degree of dissolution in the water column and/or seafloor (Berger, 1970; Van Andel et al., 1975; Lyle et al., 1995; Lyle, 2003; Pälike et al., 2012; Lyle et al., 2019). Understanding past changes in surface water productivity and deep-sea dissolution can inform about past climate development, and vice versa, how global processes affected regional production and deposition of biogenic carbonates. Primary and export productivity is a sensitive recorder of past climate variability, responding to changes in solar insolation and nutrient availability (Coxall and Wilson, 2011; Pälike et al., 2012; Lyle and Baldauf, 2015; Carter et al., 2016; Liebrand et al., 2018). Dissolution at the seafloor is primarily driven by regional changes in the carbonate compensation depth, with less carbonate preserving in areas with corrosive bottom waters (Berger, 1970; Van Andel et al., 1975; Lyle et al., 2019). Deep marine carbonate variability in the Equatorial Pacific Ocean is well-documented for the Cenozoic (Van Andel et al., 1975; Lyle, 2003; Pälike et al., 2012; Lyle and Baldauf, 2015; Kochhann et al., 2016; Beddow et al., 2018; Lyle et al., 2019). However, relatively few Atlantic records of comparable quality, resolution and extent exist (e.g., Liebrand et al., 2016), limiting our understanding of the palaeoceanographic evolution of this basin. Improving our understanding of the Southeastern Atlantic Ocean, including the Angola Basin, is of particular interest, as the water column structure and both surface and deep water ocean circulation in this strategic region has the potential to record palaeoceanographic changes in both the North Atlantic and Southern Oceans (Seidov and Maslin, 2001; Bell et al., 2015).

https://doi.org/10.5194/cp-2020-108
Preprint. Discussion started: 4 September 2020


Climate of the Past Discussions

Here, we present the first astronomically tuned record of Southeastern Atlantic carbonate deposition spanning the last 30 Myr at orbital-scale resolution. We use expanded deep-sea sedimentary sequences from Ocean Drilling Program (ODP) Sites 1264 (Leg 208; Shipboard Scientific Party Leg 208, 2004a), located on Walvis Ridge. New high-resolution X-ray fluorescence (XRF) core scanning data is collected for the mid Miocene-Present sediments at ODP Site 1264, which is integrated with published Oligocene-early Miocene XRF data from ODP Sites 1264 and 1265 (Liebrand et al., 2016). The XRF ln(Ca/Fe) data is used to verify, update and revise the composite depth scale and splice at Site 1264 to form a continuous 315.96 m record. Carbonate content (%$CaCO_3$) is estimated using the XRF ln(Ca/Fe) data. We generate an astrochronology between 3 and 17 Ma using the new %$CaCO_3$ data, which is integrated with published Oligocene-early Miocene and Plio-Pleistocene age models (Bell et al., 2014; Liebrand et al., 2016). These high-resolution, astronomically tuned carbonate records will allow us to investigate how these orbital pacing regimes relate to the broader climatic trends of the last 30 Myr.

2 Materials and Methods

2.1 ODP Sites 1264 and 1265

This study utilises material recovered at ODP Site 1264 on the Angola Basin side of Walvis Ridge in the Southeastern Atlantic (Fig. 1; 28◦31.955′S, 2◦50.730′E, 2505 m water depth; Shipboard Scientific Party Leg 208, 2004a), which was drilled during ODP Expedition 208 to provide a Cenozoic deep-sea record of the South Atlantic (Shipboard Scientific Party Leg 208, 2004a, 2004b). At Site 1264, a continuous ~316 m shipboard composite section back to the early Oligocene was developed using magnetic susceptibility and 600/450nm colour reflectance data (Shipboard Scientific Party Leg 208, 2004a). Oligocene-early Miocene XRF ln(Ca/Fe) data was used to verify the shipboard splice and produce a revised composite depth (rmcd) scale (Liebrand et al., 2016, 2018). Liebrand et al. (2016) filled four short Oligo-early Miocene core gaps at Site 1264 with data from Site 1265 (Fig 1; 28◦ 50.101′ S, 2◦ 38.354′ E, 3059 m water depth; Shipboard Scientific Party Leg 208, 2004b) to provide a continuous sedimentary sequence. Site 1264 and the relevant intervals of Site 1265 are characterised by high biogenic carbonate, with shipboard analysis indicating average $CaCO_3$ content of 92-96 weight% (Shipboard Scientific Party Leg 208, 2004a, 2004b). At 1264, shipboard linear sedimentation rates (LSR) derived from bio-magnetostratigraphy are low for the early-mid Miocene (21-12 Ma, 1-8 m/Myr) and early Plio-Pleistocene intervals (3-0 Ma, 4-8 m/Myr). LSR are higher during the Oligo-early Miocene (30-21 Ma, 6-22 m/Myr) and are highest in the late Miocene-early Pliocene (12-3 Ma), where they range between 8 and 31 m/Myr. The Oligocene-early Miocene (30-17 Ma) and Plio-Pleistocene (5.3-0.0 Ma) shipboard LSR were confirmed by previous studies on Sites 1264 and 1265 (Liebrand et al., 2011, 2016, 2017, 2018; Bell et al., 2014, 2015), which also support the shipboard notion that these sites are excellent recorders of orbital-scale climate dynamics.

https://doi.org/10.5194/cp-2020-108
Preprint. Discussion started: 4 September 2020


Climate of the Past Discussions

2.2 Core images

To assist with splice verification, astronomical tuning and data interpretation, we compiled core composite images for ODP Site 1264 from both cropped line-scan images and core table top photos using Code for Ocean Drilling Data (CODD 2.1 – www.codd-home.net; Wilkens et al., 2017). After cropping the original line scan images (JANUS – http://www-odp.tamu.edu/database/), each core section image was compiled into a composite core image and scaled to depth using the Includes_Core_Image_Assembly functions. The line scan images obtained during ODP Leg 208 "Walvis Ridge" are redder in colour than they appear in the core table top photos. This is likely an artefact of the line scanning calibration, which had only recently been introduced at the time (Fig. 1). The composite images were also compiled from lighting corrected core tabletop photos using CODD (Includes_Core_Table_Photos functions). These core tabletop composite images more realistically reflect the original colour of the cores. However, because the core box-derived composite images are exceptionally white, we use the line scan-derived composite images as they visually highlight the sedimentary cyclicity at Site 1264 better, and thus are more beneficial to evaluating and revising the composite splice together with XRF and physical property data (see Fig 2; Section 2.3 and 3.1). The composite core box/line scan core images from Site 1265 (Westerhold et al., 2017) were spliced into the four Oligo-early Miocene core gaps to form a continuous composite core image spanning the early Oligocene to present day using the Site 1264 to Site 1265 ties from (Liebrand et al., 2016), updated to accommodate any splice revisions (see also Section 3.1; Supplementary Figure 5 and Table 5).

2.3 X-ray fluorescence core scanning

XRF core scanner data were collected at ODP Site 1264 between 0-195 rmcd (revised metres composite depth) to connect with previously published XRF core scanning data spanning 195-315.96 rmcd (Liebrand et al., 2016). The new XRF data was generated in three measurement campaigns in 2013 (29.21-153.28 rmcd), 2017 (141.49-195.12 rmcd) and 2018 (0-33.35 rmcd). Ca, Fe, K, Mn, Si and Ti were measured during a 10 kV run at 1-2 cm resolution over a 1 cm^2 area with down-core slit size of 10-12 mm directly at the core surface of Site 1264 archive halves with XRF Core Scanner II/III (AVAATECH Serial No. 2/12) at the MARUM - University of Bremen. In 2018, Ba and Sr were additionally measured during a 50 kV run across intervals that proved relatively more problematic to splice. The following settings were used: 2013) MARUM XRF III, 10 kV/0.2 mA/15 s count time; 2017) MARUM XRF II, 10 kV/0.15 mA/15 s count time; 2018) MARUM XRF III, 50 kV/0. 5 mA/7 s count time/Cu filter, 10 kV/0.035 mA/7 s count time. The split core surface was covered with a 4 µm thick SPEXCerti Prep Ultralene1 foil to avoid contamination of the XRF measurement unit and desiccation of the sediment. Selected intervals were rerun during successive campaigns to account for differences in measurement intensity between datasets, including with the published Liebrand et al. (2016) data. All earlier scanned XRF data was calibrated to the 2018 dataset using an individual linear regression for each element between 2018 and 2011 (Liebrand et al., 2016), 2013 and 2017 respectively (see Supplementary Information and Supplementary Figure 1). All XRF core scanning intensity data are reported in Supplementary Table 1.

https://doi.org/10.5194/cp-2020-108
Preprint. Discussion started: 4 September 2020

Climate of the Past Discussions

2.4 XRF-derived $CaCO_3$ estimates and $CaCO_3$ MARs

Liebrand et al. (2016) showed that the XRF ln(Ca/Fe) ratio shows a strong positive correlation with shipboard coulometric $CaCO_3$ data from Site 1264 (Shipboard Scientific Party Leg 208, 2004a). We use a similar approach to generate a continuous record of $CaCO_3$ content using the combined Site 1264 XRF ln(Ca/Fe) dataset calibrated to the shipboard $CaCO_3$ data (%$CaCO_3$ = 79.642 + (2.6441 * ln(Ca/Fe)); r^2 = 0.7572; Supplementary Figure 5). This calibration is within the 2σ uncertainty of the Oligocene-early Miocene calibration used by Liebrand et al. (2016) This data was combined with the %$CaCO_3$ data from Site 1265 (Liebrand et al., 2016) to form a ~315 m/~30 Myr continuous record of $CaCO_3$ content at Walvis Ridge. Bulk and $CaCO_3$ mass accumulation rates (MARs; g/cm^2/kyr) were calculated using the following formulas:

$$MAR_{Bulk} = \rho_{dry} \times LSR \quad (1)$$

$$MAR_{CaCO_3} = \rho_{dry} \times LSR \times \left(\frac{\%CaCO_3}{100}\right) \quad (2)$$

using the LSR (cm/kyr) calculated using the new astrochronology (Section 4) and dry bulk density ρ_{dry} (g/cm^3) estimated using the shipboard gamma ray attenuation (GRA) bulk density data calibrated to the shipboard discrete dry density data (Shipboard Scientific Party Leg 208, 2004a) (Supplementary Figure 6).

3 Results

3.1 Site 1264 splice revision, off-splice mapping, and the 1264 to 1265 correlation

The line-scan composite photos and XRF data, especially the ln(Ca/Fe) and Ba data, show that there are several misalignments in sedimentary features when using the shipboard composite depth scale and splice (Fig. 2). This is especially pronounced in intervals where the shipboard physical property data was low amplitude due to very high $CaCO_3$ content, e.g., during the late Miocene-early Pliocene interval. Using the XRF ln(Ca/Fe) ratio, the shipboard splice was verified between 0 and 196.13 rmcd and revised where needed (Fig. 2, Supplementary Figure 2; Supplementary Tables 2 & 3). Where the inter-hole correlation based on the ln(Ca/Fe) ratio was ambiguous, the Ba data was used (see Supplementary Figure 2). Revisions were made between 27 and 149 rmcd, and generally resulted in changes of less than 0.6 m relative to the shipboard composite depth and splice (Supplementary Tables 2 & 3), with the exception where Hole 1264A-11 was shifted by -1.26 m relative to Hole 1264B-11 in order to improve the correlation (Fig. 2). The composite core images, and the ln(Ca/Fe) data, together with the shipboard 600/450nm colour reflectance and MS data (Shipboard Scientific Party Leg 208, 2004a) were also used to map off-splice intervals of Holes 1264A and 1264B onto the splice between 0 and 196.13 rmcd (Supplementary Table 4).

Liebrand et al. (2016, 2018) previously revised the Oligo-early Miocene interval of the composite depth scale, composite splice and mapping pairs for Site 1264, as well as the Site-to-Site correlation between Sites 1264 and 1265. The revisions in

https://doi.org/10.5194/cp-2020-108
Preprint. Discussion started: 4 September 2020


Climate of the Past Discussions

the upper sediment column result in a cumulative shift of -1.96 m to the Liebrand et al. (2016, 2018) composite depth scale/splice, mapping pairs and Site 1264 depths in the Site 1264 to Site 1265 correlation between 196.13 rmcd and 315.96 rmcd (Supplementary Tables 2-5). Furthermore, the line-scan composite core photos showed that the mapping of Core 1264B-29H to the splice, erroneously corrected in Liebrand et al. (2018) from original mapping in Liebrand et al. (2016), should be adjusted (see Supplementary Figure 3 and Table 4). The composite depth scale and splice revisions resulted in two small gaps in the Plio-Pleistocene Site 1264 isotope record (Bell et al., 2014): ~15 cm (~17 kyr) between 27.25-27.40 rmcd and ~25 cm (~11 kyr) between 54.18-54.43 rmcd.

3.2 Site 1264 $CaCO_3$ estimates and MARs

The XRF-derived $CaCO_3$ content at Site 1264 is generally high throughout, ranging between minimum values of 92% and maximum values of 97% (Fig 3). The recalibrated $CaCO_3$ content between ~205 and ~316 rmcd (early Oligocene-early Miocene) span 93-96%, which is within error of the original calibrated $CaCO_3$ content reported and discussed in detail by Liebrand et al. (2016). The lowest $CaCO_3$ content (92-93%) occur between 205 and 190 rmcd (mid Miocene). The $CaCO_3$ content especially shows clear 0.5 m cycles in this interval. $CaCO_3$ content increase slightly to 94% between 190 and 180 rmcd (mid Miocene) and then remain around 94-95% until ~118 rmcd (early late Miocene). The $CaCO_3$ content initially display short 0.6 m cycles, but after ~185 rmcd, 0.2-0.3 m cycles are superimposed upon ~1-2 m cycles. $CaCO_3$ content undergo a two-step rapid increase to 96% between ~118 and 110 rmcd and again to 97% between 105 and 10 rmcd (both latest Miocene). $CaCO_3$ content remains around 97% until 90 rmcd, after which %$CaCO_3$ remains around 96% until 40 rmcd. Between ~118 and ~40 rmcd (latest Miocene), ~1.0 m cycles and occasionally ~0.5 m cycles, are prevalent, although the amplitude of the short-term cycles is reduced compared to the deeper interval. $CaCO_3$ content slowly drop to 95% by 15 rmcd and decrease further to 93-94% in the upper 15 m of the record. Short-term cycles are less well expressed in this upper interval.

$CaCO_3$ content accounts for >90% of the sediment mass. As a result, the bulk (0.3-4.7 g/cm^2/kyr) and $CaCO_3$ (0.3-4.5 g/cm^2/kyr) MARs are remarkably similar, with trends controlled almost completely by variability in sedimentation rates (Fig 3). The Oligocene-early Miocene $CaCO_3$ MARs generally oscillate between 1-2 g/cm^2/kyr from ~315 to 205 rmcd. MARs are very low (~0.3-0.7 g/cm^2/kyr) between 205 and 190 rmcd, before slowly increasing to 1.0-2.5 g/cm^2/kyr between 190 and ~118 rmcd. The highest MARs (2.5-4.5 g/cm^2/kyr) occur between ~118 and 35 rmcd, with values decreasing back to 1-2 g/cm^2/kyr after ~35 rmcd. The highest frequency variability in the bulk and $CaCO_3$ MARs results from variability in dry bulk density (Shipboard Scientific Party Leg 208, 2004a) superimposed upon variability reflecting the changing resolution of the astrochronology.

https://doi.org/10.5194/cp-2020-108
Preprint. Discussion started: 4 September 2020

4 Depth and age models for Site 1264

4.1. Cyclostratigraphy and initial bio-/magnetostratigraphic age model

Here, we describe the imprint of cyclic patterns on the Site 1264 $CaCO_3$ content record. New cyclostratigraphy covers the upper ~205 m of the sedimentary sequence recovered at Site 1264, which corresponds to strata of middle Miocene to late Pleistocene age. Cyclostratigraphy of the lowermost ~113 m from Site 1264 (between ~205 and ~316 rmcd), which corresponds to the early Oligocene to early Miocene time interval, was previously described in great detail (Liebrand et al., 2016). A cycle interpretation and age model were also previously presented for the upper ~57 m from Site 1264 (Bell et al., 2014); however, due to several splice revisions between 27 and 55 rmcd (see Section 3.1) we briefly re-evaluate the cycle imprint on this part of the record (see Sections 4.1.3 and 4.1.4.).

The upper ~205 m is split into for intervals that are characterized by distinct cyclic patterns and/or average sedimentation rates (Sections 4.1.1., 4.1.2, 4.1.3. and 4.1.4). We apply an 11^{th} order polynomial age model computed on selected (i.e. high-quality) bio- and magnetostratigraphic depth-age points to obtain a first-order approximation of the durations of the cycles that we identify in the depth domain (see Supplementary Table 6, Supplementary Figures 7 and 8). After applying the polynomial age model, the record was tuned to generate an astrochronology (Section 4.2)

4.1.1. Depth interval between 205 and 190 rmcd

Lithological cycles broadly varying around 2 and 0.5 m length are present in the wavelet analysis of the $CaCO_3$ content for the interval between 205 and 190 rmcd (Fig 4) The bio-/magnetostratigraphic age model indicates that the LSR decreases to low values that vary around 0.5 cm/kyr. Applying this LSR to the 2 and 0.5 m cycles yield durations of approximately 405 and ~125 kyr, respectively. These durations are in very close agreement with the strong eccentricity pacing of $CaCO_3$ content cyclicity found for the underlying early Oligocene-early Miocene sediment package (Liebrand et al., 2016). We infer that eccentricity pacing of the carbonate record remained dominant from the base of Site 1264 to ~190 rmcd regardless of the changes in LSR, which were lower between 205 and 190 rmcd compared to the deeper interval (Fig 3). This interpretation is in agreement with visual inspection of the data, e.g., bundling of 110 kyr cycles in 405 kyr cycles (Fig 3, 4 and 5, panel I.a).

4.1.2. Depth interval between 190 and 115 rmcd

The depth interval between 190 and 115 rmcd is marked by cycles that gradually shift from 0.2 to 0.3 m, from about 1 to approximately 2 m, and in the range of 4 to 6 m (Fig 4). The bio-magnetostratigraphic age model indicates that these quasi-stable cyclicities in the depth domain are resultant from low, but gradually increasing LSR, that vary from ~1 cm/kyr between 190 and 160 rmcd to ~1.5 cm/kyr between 160 and 115 rmcd. Based on this initial age model we can tentatively link the 0.2 to 0.3 m cycles to precession, the 1 to 2 m cycles to ~110 kyr eccentricity and the 4 to 6 m cycles to 405 kyr eccentricity (Supplementary Figure 8). These inferred cycle durations correspond to known ratios between precession, short and long eccentricity of five precession cycles per ~110 kyr cycle, and about four ~110 kyr cycles per 405 kyr cycle. Overall

https://doi.org/10.5194/cp-2020-108
Preprint. Discussion started: 4 September 2020


Climate of the Past Discussions

the bio-/magnetostratigraphic age model suggests that the ~110-kyr eccentricity cycle is still most strongly expressed between 17 and 13 Ma, similar to the older interval between 30 and 17 Ma (see Section 4.1.1. and Liebrand et al., 2016). Strong eccentricity cycles were also noted in this interval in the equatorial Pacific (Kochhann et al., 2016). The presence of a weak 405 kyr signal in the Site 1264 $CaCO_3$ content contrasts with the Oligocene interval, for which no uniform imprint of the 405 kyr cycle on $CaCO_3$ content could be discerned (Liebrand et al., 2016).

4.1.3. Depth interval between 115 and 35 rmcd

Although detailed depth and age models are available for upper 55 rmcd of Site 1264 (Bell et al., 2014), resulting from several splice revisions (see Section 3.1.) we deem a modest re-evaluation of the cyclostratigraphy for this interval beneficial for subsequently obtaining a final tuned age model (see also Section 4.1.4.). The wavelet analysis of the $CaCO_3$ data in the stratigraphic depth domain between 115 and 35 rmcd show clear cyclicity (Fig 4). However, in comparison to the previous depth intervals the amplitude of these cycles is much reduced, and none of the cycles are statistically significant in the depth domain above the 95% level. Nevertheless, we document depth periodicities of ~0.5 m, ~1 m, 3 to 4 m, and ~10 to 12 m. From the bio-/magnetostratigraphic ages we compute average LSR of 2 to 3 cm/kyr, and tentatively infer that these periodicities in the depth domain are linked to the 20 kyr precession, the 40 kyr obliquity, and the ~110 and 405 kyr eccentricity cycles, respectively (Supplementary Figures 6 and 8). For part of this depth interval (55-35 rmcd), both $CaCO_3$ estimate data and benthic foraminiferal $\delta^{18}O$ data is available, and we visually derive an antiphase relationship between these two proxy records (Supplementary Figure 9), which aids our tuning approach for this interval (see Section 4.2.2.).

4.1.4. Depth interval between 35 and 0 rmcd

In general, clear cyclicity is hard to observe in the upper interval of the wavelet analysis of the Site 1264 $CaCO_3$ content, apart from the presence of somewhat stronger cycles with periodicities of 1.0 to 1.5 m. Visually, we are able to identify higher frequency cycles in these data, however their amplitude is not as pronounced compared to the interval between 115 and 35 rmcd. We derive averaged LSR of <1 cm/kyr for this interval based on the initial bio-/magnetostratigraphic age model. Benthic foraminiferal $\delta^{18}O$ maxima (Bell et al., 2014) coincide with $CaCO_3$ content minima, however this phase relationship is not well-defined throughout this interval and becomes less clear at the top of the record. Based on the initial age model we note absence of clear precession and obliquity paced cyclicity in both benthic foraminiferal $\delta^{18}O$ and $CaCO_3$ content records during the last 2.5 Ma (Supplementary Figure 8). The 1.0 to 1.5 m periodicity is probably linked to either the ~110-kyr eccentricity paced cycles or the main ice age cycles of the middle and late Pleistocene. This would indicate a change in response of both benthic foraminiferal $\delta^{18}O$ and $CaCO_3$ content during this time interval, in line with the evolution of the global cryosphere and climate systems during this time.

https://doi.org/10.5194/cp-2020-108
Preprint. Discussion started: 4 September 2020


Climate of the Past Discussions

4.2. Astronomically tuned age model

Two published astrochronologies exist for Sites 1264/1265: 1) an Oligo-early Miocene one between 30 and 17 Ma based on tuning %$CaCO_3$ to eccentricity (Liebrand et al., 2016); and 2) a Plio-Pleistocene one spanning 5.3 to 0 Ma based on correlating the Site 1264 benthic foraminiferal $\delta^{18}O$ record to the LR04 Plio-Pleistocene benthic $\delta^{18}O$ stack (Lisiecki and Raymo, 2005; Bell et al., 2014). The Bell et al. (2014) chronology has to be re-evaluated in the early Pliocene, especially prior to 3.5 Ma (~27 rmcd), resulting from the splice revisions between 27 and 149 rmcd at Site 1264. The Oligocene to early Miocene astrochronology remains unchanged, but the depth-age tie points were updated to accommodate the -1.96 m cumulative depth scale shift due to depth model/splice revisions in the overlying sedimentary sequence. The cyclostratigraphic analyses indicate that the combined Site 1264/1265 %$CaCO_3$ record is suitable for developing an astrochronology for the interval 17-3.5 Ma (see Section 4.1). However, because of the variable orbital forcing imprint recorded at Site 1264, it was not possible to implement a single and uniform tuning strategy to the entire record. In all, three distinct strategies were employed to achieve a 30 Myr astrochronology for Site 1264 (Supplementary Table 7):

I) 30-8.0 Ma: $CaCO_3$ content to eccentricity, with obliquity also used in 2.4 Myr minima when stable in the solution:
   I.a) 30-9.7 Ma: $CaCO_3$ content to eccentricity (visually aided by $\delta^{18}O$, where available)
   I.b) 9.7-8.0 Ma: $CaCO_3$ content to E(T)
II) 8.0-3.3 Ma: $CaCO_3$ content (/benthic $\delta^{18}O$) to ET-P
III) 3.3-0.0 Ma: benthic $\delta^{18}O$ to LR04

4.2.1 early Oligocene-late Miocene (30.0-8.0 Ma)

Liebrand et al. (2016) showed that between 30-17 Ma $CaCO_3$ content maxima coincide with benthic $\delta^{18}O$ maxima, which in turn have an inverse relationship with the ~110 kyr eccentricity components (e.g. the ~95 and ~125 kyr cycles). They generated an astrochronology by tuning $CaCO_3$ content minima to eccentricity maxima (see Liebrand et al., 2016 for details). The variability and dominant cyclicity in $CaCO_3$ content for the 17-8 Ma interval are comparable to the 30-17 Ma interval (see Section 4.3.1 and 4.3.2). We therefore consider the inverse phase relationship between $CaCO_3$ content and ~110 kyr eccentricity to be valid across the 30-8 Ma interval and tune $CaCO_3$ content minima to Eccentricity maxima (La2004) (Fig 5). Benthic foraminiferal stable isotope records are not currently available between 17-8 Ma. Future work can independently test the Miocene stability until 8 Ma of the Oligo-early Miocene derived phase relationship between $CaCO_3$ content and ~110 kyr eccentricity.

Our tuning strategy is very robust where the amplitude modulation of ~110 kyr eccentricity is high; however, the amplitude of the ~110 kyr eccentricity cycles are more muted during 2.4 Myr eccentricity minima (~17.0-16.6 Ma, ~14.6-14.2 Ma, ~12.6-12.2 Ma, ~9.7-9.3 Ma). Obliquity becomes more prevalent in these 2.4 Myr eccentricity minima and can act as an alternative tuning target when ~110 kyr eccentricity amplitude is reduced. However, because of uncertainties in past changes to tidal dissipation and dynamical ellipticity, the exact phase of obliquity is not known prior to 10 Ma (Lourens et

https://doi.org/10.5194/cp-2020-108
Preprint. Discussion started: 4 September 2020


Climate of the Past Discussions

al., 2004; Zeeden et al., 2013, 2014). We therefor apply two slightly adapted approaches of the Liebrand et al. (2016) tuning strategy to the 17-8 Ma interval:

I.a) From 17-9.7 Ma, we tune $CaCO_3$ content minima to E maxima (La2004; Laskar et al., 2004), with an uncertainty better than ±50 kyr. This uncertainty increases to up to ±100 kyr in the 2.4 Myr minima at ~17.0-16.6 Ma, ~14.6-14.2 Ma, ~12.6-12.2 Ma (Fig 5, Panel Ia).

I.b) From 9.7-8.0 Ma, we tune $CaCO_3$ content minima to E(T) maxima (La2004; Laskar et al., 2004). Generally, the $CaCO_3$ content minima are tuned to E maxima, with an uncertainty better than ±50 kyr. During the 2.4 Myr eccentricity minima ~9.7-9.3 Ma, $CaCO_3$ content minima are tuned to ET maxima (uncertainty up to ±40 kyr; Fig 5, Panel I.b).

We chose to tune to the La2004 solution (Laskar et al., 2004), as over the last 30 Myr the eccentricity components are essentially identical to the La2011_ecc3L solution (Laskar et al., 2011) used in Liebrand et al. (2016). Furthermore, only the La2004 has the obliquity solution used in I.b) approach. The cyclostratigraphic analyses show that precession cycles are also imprinted in the record younger than 14 Ma, so there was potential to develop an astrochronology at precession-level. However, as uncertainties in past tidal dissipation and dynamical ellipticity mean the phase of precession is also uncertain older than 10 Ma (Lourens et al., 2004; Zeeden et al., 2013), we were conservative in tuning to eccentricity only prior to 9.7 Ma.

4.2.2 late Miocene-mid Pliocene (8.0-3.3 Ma)

The strong ~110 kyr eccentricity imprint on the $\%CaCO_3$ record is significantly reduced after 8 Ma. Spectral analyses show that obliquity and precession are more prevalent after 8 Ma until around 2.5 Ma. We apply a different tuning strategy between 8.0-3.3 Ma, because the prevalent cyclicity in the $\%CaCO_3$ data changes from eccentricity/precession-driven (older than 8 Ma) to obliquity/precession-driven (younger than 8 Ma) (see Section 4.1). A change in the relationship between the benthic $\delta^{18}O$ and $\%CaCO_3$ data in the Plio-Pleistocene compared to the Oligo-early Miocene also indicates that a change in tuning approach is warranted. Where overlapping benthic $\delta^{18}O$ and $\%CaCO_3$ is available (5.3-3.3 Ma; Bell et al., 2014), the two proxies show an inverse relationship, with the obliquity- and precession-driven $CaCO_3$ content minima coinciding with benthic $\delta^{18}O$ maxima. This contrast to the positive relationship these proxies display in the Oligocene-early Miocene with the 110-kyr eccentricity-driven $CaCO_3$ content minima coinciding with benthic $\delta^{18}O$ minima (Liebrand et al., 2016). The phase relationship between benthic $\delta^{18}O$ and obliquity is well established for this time interval, with benthic $\delta^{18}O$ minima tuned to obliquity maxima (Shackleton et al., 1996; Shackleton and Hall, 1997; Hodell et al., 2001; Zeeden et al., 2013; Drury et al., 2017, 2018b). Considering the inverse benthic $\delta^{18}O$-$CaCO_3$ content relationship after 5.3 Ma, we assume that $CaCO_3$ content maxima correlate to obliquity maxima for the entire interval 8 to 3.3 Ma. Precession and obliquity are the two prevalent cyclicities present in both the $CaCO_3$ content and benthic $\delta^{18}O$ data. The interference pattern observed in both datasets is most similar to an ET-P solution. As such, we generated an astrochronology by tuning $CaCO_3$ maxima to ET-P maxima (i.e., Southern Hemisphere insolation minima) (uncertainty up to ±10 kyr), guided by benthic $\delta^{18}O$ where these are available (Fig 5, Panel II). Based on the shipboard biostratigraphy, there was some indication that there might be an unconformity of ~0.6

https://doi.org/10.5194/cp-2020-108
Preprint. Discussion started: 4 September 2020


Climate of the Past Discussions

Myr in the late Miocene at the base of Core 1264A-7H (~76-77 rmcd) (Shipboard Scientific Party Leg 208, 2004a). However, we find excellent agreement between the $CaCO_3$ content and the ET-P solution, with 80 and 75 rmcd correlating well with 6.3-6.1 Ma (Fig 5, Panel II).

4.2.1 mid Pliocene-Pleistocene (3.3-0.0 Ma)

Because no changes were made to the shipboard splice in the upper 27 rmcd (3.5 Myr), we could use the original Bell et al. (2014) age model in this interval. The Bell et al. (2014) age model was generated by correlating a benthic foraminiferal $\delta^{18}O$ stack comprising data from ODP Sites 1264 and 1267 to the LR04 $\delta^{18}O$ stack (Lisiecki and Raymo, 2005). We confirmed the Bell et al. (2014) age model by comparing the Site 1264 $\delta^{18}O$ record to the equatorial Atlantic CR17 $\delta^{18}O$ stack (Wilkens et al., 2017), which has an independent tuning based on MS and lightness. The agreement between the two $\delta^{18}O$ records is very good (Fig 5, Panel III), which further supports the accuracy of the original Bell et al. (2014) age model in this interval.

5 Discussion

5.1 History of South Atlantic $CaCO_3$ deposition and its changing orbital pacing since the Oligocene

Previous work at ODP Site 1264 shows that the recovered sediments are an excellent recorder of Southeast Atlantic orbital climate variability for the last 30 Myr (Shipboard Scientific Party Leg 208, 2004a; Bell et al., 2014, 2015; Liebrand et al., 2016). Oligocene to early Miocene carbonate and benthic $\delta^{18}O$ records from Site 1264 showed that the early icehouse was dominated by large ~110 kyr eccentricity driven variability in the Antarctic ice sheet (Liebrand et al., 2016, 2017). By the Pliocene, the south Atlantic Site 1264 was heavily influenced by North Atlantic Deep Water (NADW) (Bell et al., 2014, 2015). The new continuous depth (~316 m; Section 3.1) and age (~30 Myr; Section 4) model presented here for the entirety of Site 1264 constitutes a reference framework for future palaeoclimatic and palaeoceanographic studies. Furthermore, the new data (Fig 6) allows for the unprecedented investigation of how long-term climate trends and orbital-scale climate variability have impacted this region, especially for the interval between 17 and 5 Ma, for which no high-resolution Southeast Atlantic records previously existed.

At Site 1264, $CaCO_3$ content remains very high, with all long- and short-term variability occurring between 92-97.5% $CaCO_3$ (Fig 6). Carbonate content varies between about 92-96% during the Oligocene to early late Miocene (30-8 Ma). The lowest $CaCO_3$ content (92-93.5%) and MARs (~0.3-0.7 g/cm^2/kyr) occur between ~18.5-14.4 Ma, which broadly coincides with the Miocene Climatic Optimum (MCO; 17-14.7 Ma; Shevenell et al., 2004; Holbourn et al., 2005) (see Section 5.2 for discussion). Carbonate varied between 94-96% during the Oligocene-early Miocene (30-18.5 Ma; Liebrand et al., 2016) and the early late Miocene (14.4-8.0 Ma), coincident with MARs of ~1-2.5 g/cm^2/kyr. The highest $CaCO_3$ content (96-97.5%) and MARs (2.5-4.5 g/cm^2/kyr) are found between 8-4 Ma (Fig 6), indicating high carbonate productivity coincident with the known age of the global Late Miocene Biogenic Bloom (LMBB; Lyle et al., 2019) (see Section 5.3 for discussion).

https://doi.org/10.5194/cp-2020-108
Preprint. Discussion started: 4 September 2020


Climate of the Past Discussions

The influence of the long 405 kyr eccentricity on $CaCO_3$ deposition at Site 1264 is complicated. Liebrand et al. (2016) could not observe a uniform imprint of the 405 kyr cycle on $CaCO_3$ content during the Oligocene interval at Site 1264. This contrasts with the clearer imprint of a 405 kyr cycle on $CaCO_3$ deposition during the Miocene between ~21-5 Ma. We can recognise three distinctly different orbital imprints on the short-term $\%CaCO_3$ variability (Fig 6):

1) ~110 kyr eccentricity prevails as the dominant forcing between 30 and ~13 Ma;
2) Precession-driven $\%CaCO_3$ oscillations appear ~14-13 Ma, and pace the main short-term variability until ~8 Ma;
3) Obliquity becomes the significant driver at Site 1264 after ~7.7 Ma, and together with precession imprints a characteristic interference pattern on $\%CaCO_3$;

Although different tuning strategies are used to generate a continuous astrochronology (see Section 4.2), these shifts are also visible in the depth and bio- and magnetostratigraphic age model spectra (see Section 4.1), indicating they are independent of the changes in tuning strategy.

The three pacings observed in the Southeastern Atlantic $CaCO_3$ deposition broadly coincide with major developments in climate, the cryosphere and/or the carbon cycle. The strong expression of ~110 kyr eccentricity-driven $\%CaCO_3$ variability at Site 1264 between 17-13 Ma is in line with the dominant $\%CaCO_3$ variability at Site 1264 during the Oligo-early Miocene (30-17 Ma; Fig 6; Liebrand et al., 2016). This is in line with that the Oligocene to mid Miocene unipolar ice house climate was predominantly paced by short-term eccentricity during widespread global warmth (Pälike et al., 2006; Tian et al., 2013; Holbourn et al., 2014, 2015; Beddow et al., 2016, 2018; Kochhann et al., 2016; Liebrand et al., 2016, 2017; Voigt et al., 2016). However, the orbital imprint on $CaCO_3$ content shifts between 14 and 13 Ma, with eccentricity-modulated precession cycles progressively becoming more clearly superimposed on the larger ~110 kyr cycles. This shift occurs after global cooling and the reglaciation of Antarctica across the mid-Miocene Climate Transition (~13.9 Ma; mMCT; Holbourn et al., 2005). Some precession-driven $\%CaCO_3$ cycles are previously observed at Site 1264 between 23.5-19.5 Ma, superimposed on larger ~110 kyr eccentricity cycles (Fig 6; Liebrand et al., 2016). However, the ~110 kyr eccentricity cycles are greater in amplitude than the precession cycles. In contrast, concurrent with the increase in precession power in the $\%CaCO_3$ data after 14 Ma, we observe a decrease in strength of the ~110 kyr eccentricity cycles (Fig 6). During the 2.4 Myr eccentricity minima from ~12.6-12.2 Ma and ~9.7-9.3 Ma, the precession imprint is muted, and obliquity paces $\%CaCO_3$ variability.

Although some power remains in the ~110 kyr eccentricity bandwidth, the orbital imprint on $\%CaCO_3$ variability changes around 7.7 Ma to a strong obliquity-precession interference pattern, which remains visible until ~3.3 Ma (Fig 5 and 6). The onset of prevalent obliquity-precession pacing that we observe after ~7.7 Ma in the Site 1264 $\%CaCO_3$ record has been observed globally in benthic $\delta^{18}O$ records and is associated with increased influence of high-latitude processes (Drury et al., 2017, 2018b; Holbourn et al., 2018). Although benthic $\delta^{18}O$ data are not available at Site 1264 between 8.0-5.3 Ma, the obliquity-precession interference pattern is visible in the benthic $\delta^{18}O$ record between 5.3 and 3.3 Ma (Fig 5). Relative to the Oligocene-early late Miocene, the amplitude of the variability is reduced during the latest Miocene and early Pliocene. Concurrent with the waning influence of ~110 kyr eccentricity at Site 1264, the highest $\%CaCO_3$ values (96-97.5%) of the

https://doi.org/10.5194/cp-2020-108
Preprint. Discussion started: 4 September 2020


Climate of the Past Discussions

entire record occur between 8 and 4 Ma. The influence of the complex late Miocene climate system on carbonate deposition is discussed in Section 5.3.

The short-term orbital imprint is more difficult to characterise after 3.3 Ma. The wavelet analysis show that ~110 kyr eccentricity influence increases in the Plio-Pleistocene compared to the latest Miocene (Fig 6). The influence of some obliquity and precession forcing on $\%CaCO_3$ remains until ~0.9 Ma, when the ~110 kyr eccentricity pacing characteristic of the middle Pleistocene appears after the Mid Pleistocene Transition (MPT; Bell et al., 2014). Compared to Site 1264, the transition from ~40 kyr to ~110 kyr pacing is recorded more clearly visible in the benthic $\delta^{18}O$ data, composite core photos and physical property data at nearby Site 1267 (physical property data from Shipboard Scientific Party Leg 208, 2004c; benthic $\delta^{18}O$ data from Bell et al., 2014; composite core photos from Westerhold et al., 2017). This difference in expression of the MPT may partly relate to water depth differences between the sites, as the deeper Site 1267 (4356 m water depth) may record a stronger deep-water signal compared to Site 1264 (2507 m water depth). However, although the onset of the Pleistocene 100-kyr cycles is not exceptionally clear at Site 1264, it is apparent that these cycles only appear after 0.9 Ma at both Sites 1264 and 1267 (Fig 6), which is considerably later than has been seen in the eastern equatorial Pacific, where 100-kyr cycles first appear in carbonate records at 1.6 Ma (Lyle et al., 2019).

Benthic foraminiferal $\delta^{18}O$ records are only available for the Oligocene-early Miocene (30-17 Ma; Liebrand et al., 2011, 2016) and the Plio-Pleistocene (5.3-0.0 Ma; Bell et al., 2014). It is therefore not yet possible to track the evolution of the relationship between the climate-cryosphere system (encompassed by benthic $\delta^{18}O$) and South Atlantic carbonate deposition over the last 30 Myr. However, in contrast to the in-phase $\%CaCO_3$-benthic $\delta^{18}O$ relationship on ~110-kyr eccentricity periodicities between 30 and 17 Ma (Liebrand et al., 2016), the new Site 1264 $\%CaCO_3$ data has an inverse relationship on obliquity periodicities with benthic $\delta^{18}O$ for the last 5.3 Myr (Fig 5; Supplementary Figure 9). This points at a considerably different relationship between the cryosphere and controls on carbonate deposition at Site 1264 in the Plio-Pleistocene and the Oligocene-early Miocene. The in-phase Oligocene to early Miocene $\%CaCO_3$-benthic $\delta^{18}O$ relationship observed at Site 1264 has been seen elsewhere for the Oligocene through to the mid Miocene, including across the mMCT (Holbourn et al., 2014, 2015; Kochhann et al., 2016; Liebrand et al., 2016; Beddow et al., 2018; Tian et al., 2018). Considering the three phases with distinctly different orbital controls on $CaCO_3$ deposition at Site 1264, it is possible that the $\%CaCO_3$-benthic $\delta^{18}O$ relationship changed from in-phase on 110-kyr eccentricity periodicities to anti-phase on obliquity periodicities concurrent with the ~7.7 Ma shift in $CaCO_3$ deposition from a predominantly eccentricity/precession-paced system to one that is more controlled by obliquity/precession. Such an interpretation would further support the notion that the Earth's system underwent a major shift in its response to orbital forcing in the late Miocene-early Pliocene (Turner, 2014; Drury et al., 2017, 2018b).

5.2 Eccentricity-Precession switch, low $\%CaCO_3$ deposition and the early-mid Miocene warmth

The early-mid Miocene marks a warm interval where Antarctic ice volume underwent major change and climatic trends deviated from the overall Cenozoic icehouse cooling pattern (Miller et al., 1991; Shevenell et al., 2004; Holbourn et al.,

https://doi.org/10.5194/cp-2020-108
Preprint. Discussion started: 4 September 2020


Climate of the Past Discussions

2005, 2014, 2015; Tian et al., 2013, 2014; Super et al., 2018). The Miocene Climatic Optimum (MCO; defined in the benthic foraminiferal $\delta^{18}O$ as between 17 and 14.7 Ma; Holbourn et al., 2015), was characterised by pervasive global warmth and more humid conditions, together with lower meridional temperature gradients and greatly reduced continental ice sheets on Antarctica compared to the present-day (Lear et al., 2000, 2015; Billups and Schrag, 2002; Shevenell et al., 2004; John et al., 2011; Pound et al., 2012; Gasson et al., 2016; Levy et al., 2016). Distal marine records that track variations in land ice volume and deep-sea temperatures are marked by a strong ~110 kyr eccentricity pacing, coupled with large 400-kyr driven carbon cycle perturbations (Monterey Excursions) (Shevenell et al., 2008; Holbourn et al., 2014, 2015; Tian et al., 2014; Kochhann et al., 2016; Ohneiser and Wilson, 2018). The MCO warmth, ice volume decrease and carbon cycle perturbations have been hypothesized to be driven by increased atmospheric CO_2 levels associated with volcanic degassing from the Columbia River Flood Basalts, with the earliest eruptions occurring after ~17.2 Ma (Foster et al., 2012; Barry et al., 2013; Greenop et al., 2014; Kasbohm and Schoene, 2018; Moore et al., 2018, 2020; Super et al., 2018; Cahoon et al., 2020; Sosdian et al., 2020). The warm MCO conditions were reversed ~13.9 Ma during the mMCT when major continental ice sheets reappeared on Antarctica associated with a large decrease in atmospheric CO_2 and global temperatures (Shevenell et al., 2004; Holbourn et al., 2005; Foster et al., 2012; Pound et al., 2012; Badger et al., 2013; Lear et al., 2015; Gasson et al., 2016; Levy et al., 2016; Super et al., 2018, 2020).

Benthic foraminiferal $\delta^{18}O$ records are not available at Site 1264 for this interval, so it is not possible to recognise the MCO at Site 1264 using this dataset. Nonetheless, the lowest $\%CaCO_3$ content (92-93.5%), which display strong ~110 kyr eccentricity pacing, and $CaCO_3$ MARs (~0.3-0.7 g/cm^2/kyr) occur between ~18.5-14.4 Ma, and broadly coincide with the MCO (Fig 6C and 7C). Little change in detrital MARs (bulk–$CaCO_3$ MARs), Si and K intensity indicates that biogenic silica and detrital input remains relatively constant and minimal across this interval. These low $\%CaCO_3$ content therefore indicate increased dissolution or decreased productivity at Site 1264, rather than dilution. The recovery of $\%CaCO_3$ content ~14.5 Ma especially agrees well with the end of the MCO ~14.7 Ma (Holbourn et al., 2015). However, at Site 1264, the decreasing $CaCO_3$ content start ~18.5 Ma, which is ~1.5 Myr before the decrease in benthic $\delta^{18}O$ normally associated with the onset of the MCO (Fig 6). During the early-mid Miocene, low $\%CaCO_3$ and $CaCO_3$ MARs were observed at multiple sites (DSDP 574; IODP U1335-U1338) in the eastern equatorial Pacific Ocean (EEP), initially decreasing after 18-17.5 Ma, and recovering to early Miocene values by 15-14.5 Ma (Piela et al., 2012; Kochhann et al., 2016). Multiproxy evidence at these EEP sites indicates that the low $\%CaCO_3$ and $CaCO_3$ MARs values were associated with increased deep-sea dissolution rather than decreased productivity, with the peak dissolution occurring at the onset of the MCO (Piela et al., 2012; Kochhann et al., 2016). The dissolution has been associated with elevated atmospheric pCO_2, increased carbon storage in the deep ocean and shoaling of the carbonate compensation depth during the early-mid Miocene global warmth (Pälike et al., 2012; Piela et al., 2012; Kochhann et al., 2016).

Assuming that the low $CaCO_3$ content and MARs at Site 1264 also reflect increased carbonate dissolution rather than a reduction in carbonate rain, there is evidence that carbonate dissolution preceded the MCO by ~1.5 Myr in the Southeastern Atlantic (Site 1264) and ~1.0-0.5 Myr in the equatorial Pacific (Piela et al., 2012; Kochhann et al., 2016). Few early-mid

https://doi.org/10.5194/cp-2020-108
Preprint. Discussion started: 4 September 2020


Climate of the Past Discussions

Miocene atmospheric CO_2 or sea surface temperatures (SST) records extend back to 18.5 Ma, but long-term trends in early-mid Miocene TEX_{86}-derived SSTs from the North Atlantic Ocean indicate that SSTs may have been at MCO-levels since ~20 Ma (Super et al., 2018; Fig 7A). It is not yet clear whether elevated SSTs prior to the MCO are a global phenomenon. However, the likely dissolution-induced lows in Southeastern Atlantic and equatorial Pacific $CaCO_3$ deposition up to ~1.5 Myr before the MCO, may indicate that the MCO itself was preconditioned by elevated temperatures and atmospheric pCO_2.

Shortly after the MCO, the overall Cenozoic cooling trend resumes across the mMCT with the reappearance of large ice sheets on Antarctica around 13.9 Ma. At Site 1264, the $\%CaCO_3$ values increase after ~14.5 Ma, which could reflect decreased deep-sea dissolution and/or increased surface-ocean productivity. Between 14 and 13 Ma, the orbital imprint on $CaCO_3$ at Site 1264 progressively shifts from ~110 kyr eccentricity-dominated pacing to precession-dominated pacing superimposed on the ~110 kyr eccentricity cycles (Fig 7C). In comparison to the Oligocene-early Miocene, the ~110 kyr eccentricity cycles are more muted, and the precession cycles are higher amplitude and more clearly expressed during the mid-late Miocene (Fig 6). The change in orbital imprint at Site 1264 after the mMCT may indicate that productivity in this region became more sensitive to precession forcing following changes to ocean circulation and/or the hydrological cycle driven by the reglaciation of Antarctica, global cooling and increased meridional temperature gradients. However, this shift also occurs after the MCO, which is characterised at Site 1264 by low LSR and MARs that may also be indicative of increased carbonate dissolution. If dissolution is the dominant control on $CaCO_3$ content at Site 1264, the increased preservation of precession cycles at Site 1264 after 14 Ma (i.e., after the mMCT) could also reflect a shift in deep-water circulation patterns bringing cooler, less corrosive deep-waters to Site 1264, allowing for the better preservation of precession-driven productivity cycles than during the middle Miocene.

5.3 Late Miocene-early Pliocene Biogenic Bloom

The latest Miocene (~8-5.3 Ma) is a complicated and dynamic interval when climate and ecosystems recognisable to the present-day first appeared (Herbert et al., 2016). There is abundant sedimentary and geochemical evidence for a global and long-lasting increase in primary productivity in the global surface ocean during the late Miocene to early Pliocene (Farrell et al., 1995; Dickens and Owen, 1999; Diester-Haass et al., 2002, 2005). This event is referred to as the Late Miocene-early Pliocene Biogenic Bloom (LMBB; Lyle et al., 2019) and has been recognised between ~8 and 4 Ma in upwelling and oligotrophic areas of all major oceanic basins (Kroon et al., 1991; Dickens and Owen, 1999; Hermoyian and Owen, 2001; Diester-Haass et al., 2002, 2004, 2005; Grant and Dickens, 2002; Liao and Lyle, 2014; Lyle and Baldauf, 2015; Lyle et al., 2019). At Sites 1264/1265, the highest $CaCO_3$ content (96-97.5%) occur between ~8 and 4 Ma and the highest bulk and $CaCO_3$ MARs (~2-4.5 g/cm^2/kyr) are found between ~7.8 and 3.3 Ma (Fig. 6 and 8C), which falls within the broad timing associated with the LMBB. As $\%CaCO_3$ is so high at Site 1264, $CaCO_3$ MARs account for most of the variability in the bulk MARs. Similarly, Lyle et al. (2019) showed that the LMBB is expressed between ~8 and 4.4 Ma in the bulk and $CaCO_3$ MAR of 6 sites in the eastern equatorial Pacific (EEP), with $CaCO_3$ MARs accounting for most of the bulk MAR variability (Fig 8D). Despite the influence of palaeogeographical heterogeneity on the absolute EEP MARs, it becomes apparent after

https://doi.org/10.5194/cp-2020-108
Preprint. Discussion started: 4 September 2020


Climate of the Past Discussions

normalisation that common productivity patterns are visible across the EEP (Lyle et al., 2019; Fig 8B and D). The Site 1264 $CaCO_3$ MARs are generally higher than the EEP sites (Fig. 8C and D), except for ODP Sites 849 and 850, which are the two highest sedimentation EEP sites (Lyle et al., 2019).

The exact cause of the LMBB is poorly understood, however key hypotheses suggest the increased primary productivity was caused by 1) increased nutrient input into the surface ocean through increased weathering/dust input and/or 2) changes to the global distribution of nutrients through changes in atmospheric and oceanic circulation patterns. The widespread documentation of the LMBB shows that the expression and timing is regionally variable (Liao and Lyle, 2014; Lyle et al., 2019; Sutherland et al., 2019). However, most of these records are low-resolution and insufficient for accurately constraining regional differences, which means we cannot yet distinguish between global changes to the nutrient budget and changes to the regional distribution of nutrients in the ocean (e.g., changes in ocean circulation and/or upwelling). The availability of orbital-scale $\%CaCO_3$ and MARs from Site 1264 and the EEP provide the opportunity to compare the LMBB at high-resolution for the first time. Based on increased $CaCO_3$ MARs, the timing of the LMBB at Site 1264 and the EEP generally agrees well (Fig 8B), which corroborates the global nature of the LMBB. After increasing from 8 Ma onwards, MARs peak between 7.2-6.6 Ma at both Walvis Ridge and the equatorial Pacific (Fig. 8B), which supports a global LMBB optimum occurring between ~7.0-6.4 Ma (Lyle and Baldauf, 2015; Lyle et al., 2019). Site 1264 also has the highest absolute $\%CaCO_3$ values at this time, indicating high productivity of carbonate producers at this time (Fig 6 and 8A). However, the LMBB extends to 3.3 Ma at Site 1264, in contrast to the western EEP, where the LMBB ends ~4.4 Ma (Fig 8B). In the far eastern equatorial Pacific near South America, high $CaCO_3$ MARs continue to ~3 Ma (Figure 8 in Lyle et al., 2019), which is further evidence for regional variability of the termination of the LMBB production interval. The recognition of global patterns and temporal heterogeneity in the expression of the LMBB between the Pacific and the Southeast Atlantic could reflect different regional responses to a single climatic forcing and/or multiple driving forces.

Constraining which primary producers drove the LMBB at different regions will be useful for disentangling regional and global patterns. The new Site 1264 $\%CaCO_3$ data has an inverse relationship with the low-resolution record of the percent >63 μm coarse fraction (%CF) during the late Miocene-early Pliocene (Keating-Bitonti and Peters, 2019; adapted to this study's new composite depth and age model; Fig 6C and 8A). Specifically, the %CF shows the opposite trend to $\%CaCO_3$ across the LMBB: decreasing %CF from 8 Ma, with the lowest %CF values occurring ~7 Ma, in line with the maximum values in $\%CaCO_3$. This inverse relationship indicates that the LMBB was predominantly driven by a change in the calcareous phytoplankton (coccolithophores) versus foraminifera ratio at Site 1264. Based on Si intensity, there is no evidence that biogenic silica producers play a major role in the LMBB at Site 1264 (Fig. 6). This contrasts to the EEP, which is upwelling dominated and where a combination of calcareous (coccolithophores) and siliceous (diatoms) phytoplankton drove the LMBB (Lyle and Baldauf, 2015; Lyle et al., 2019).

Although we cannot yet accurately distinguish global increases in nutrient delivery to the ocean versus the regional redistribution of nutrients causing localised increased primary productivity, we can consider links between this prolonged productivity event and the dynamic changes observed during late Miocene. Terrestrial and sea surface temperatures

https://doi.org/10.5194/cp-2020-108
Preprint. Discussion started: 4 September 2020


Climate of the Past Discussions

decreased rapidly during the late Miocene cooling between ~7.0-5.4 Ma (Pound et al., 2011, 2012; Herbert et al., 2016). Conversely, there is no major late Miocene increase in benthic $\delta^{18}O$ records relative to those seen mid Miocene and Pleistocene, indicating that there was no large expansion in continental ice sheet extent or substantial deep-sea cooling (Hodell et al., 2001; Drury et al., 2016, 2018b; Holbourn et al., 2018; Tian et al., 2018). The carbon cycle underwent major change in the atmospheric, terrestrial and marine realms, with evidence for an atmospheric pCO_2 decrease around ~8-7 Ma (Bolton and Stoll, 2013; Herbert et al., 2016; Mejía et al., 2017), the rise of terrestrial C_4 plants on land (Cerling et al., 1997; Behrensmeyer et al., 2007; Uno et al., 2016; Tauxe and Feakins, 2020), and the globally synchronous marine late Miocene carbon isotope shift (LMCIS; ~7.5-6.9 Ma) linked to global changes in oceanic circulation (Haq et al., 1980; Hodell and Venz-Curtis, 2006; Reghellin et al., 2015, 2020; Drury et al., 2017, 2018a).

At Site 1264, the onset of elevated $CaCO_3$ MARs (~7.8 Ma) roughly coincides with the shift from eccentricity-precession pacing to pervading obliquity-precession pacing of $\%CaCO_3$, which infers an increased influence of high-latitude processes at Site 1264 (Fig. 6). The onset of strong obliquity pacing is also observed ~7.7 Ma as asymmetric (i.e., sawtooth-shaped) benthic $\delta^{18}O$ cycles, which have a characteristic "interglacial-glacial" anti-phase relationship with benthic $\delta^{13}C$ on obliquity timescales (Drury et al., 2017). The appearance of strong obliquity forcing in multiple systems implies increased influence of high-latitude processes shortly after 8 Ma. This increased high-latitude influence may be caused by the late Miocene cooling, which was especially pronounced in the high latitudes and reached near-modern gradients around 5.4 Ma (Pound et al., 2012; Herbert et al., 2016). There is also ice-proximal evidence for enhanced glacial activity in both the Northern and Southern Hemispheres potentially indicating early transient bipolar cryosphere activity (Connell et al., 1996; Fronval and Jansen, 1996; Wolf-Welling et al., 1996; Kong et al., 2010; Williams et al., 2010). Increased glacial weathering after 8 Ma may have contributed to the onset of the LMBB through increased the nutrient influx into the ocean. An increased nutrient flux may also be driven by enhanced chemical weathering through Himalayan uplift and the intensification of the Indian and Asian Monsoon systems in the latest Miocene (Kroon et al., 1991; Filippelli, 1997; Zhisheng et al., 2001; Holbourn et al., 2018; Yang et al., 2019). Finally, the LMBB may be partly driven by increased nutrient input into the ocean as a result of widespread continental aridification coupled with trade wind intensification due to greater meridional gradients during the late Miocene cooling (7-5.4 Ma) (Hovan, 1995; Filippelli, 1997; Diester-Haass et al., 2006; Tipple and Pagani, 2007; Lyle et al., 2008; Pound et al., 2012; Herbert et al., 2016).

Regional variability in the LMBB may in turn be driven by regional differences in the extent of late Miocene cooling (Pound et al., 2012; Herbert et al., 2016), as well as regional diachrony in aridification (Molnar, 2005; Schuster et al., 2006; Lyle et al., 2008; Dupont et al., 2013). The LMCIS (~7.5-6.9 Ma) has been linked to the onset of near modern thermohaline circulation with NADW percolating further into the South Atlantic (Hodell and Venz-Curtis, 2006; Drury et al., 2017; Keating-Bitonti and Peters, 2019). A major shift in oceanic circulation would likewise affect the redistribution of nutrients around the globe, thereby potentially contributing to regional differences in nutrient supply. All these aspects go some way in explaining why the LMBB began after ~8 Ma; however, it is unclear why the LMBB continued into the Pliocene, and

https://doi.org/10.5194/cp-2020-108
Preprint. Discussion started: 4 September 2020


Climate of the Past Discussions

especially why it continued until 3.3 Ma at Site 1264. Further work disentangling global versus regional productivity patterns will be needed in future to explore causal links in greater detail.

6 Conclusions

We present a continuous Site-1264-encompassing depth (~316 m) and age (~30 Myr) model that constitutes a reference framework for future palaeoclimatic and palaeoceanographic studies. To this aim, we generated new high-resolution (1-2 cm) XRF records between 17 and 0 Ma at ODP Site 1264 in the Southeastern Atlantic. We used the XRF data to revise the shipboard composite splice, especially in the late Miocene-early Pliocene interval. The new ln(Ca/Fe) records were integrated with previously published Oligocene-early Miocene XRF records and calibrated to shipboard $\%CaCO_3$ data to obtain the first continuous Southeastern Atlantic carbonate record spanning the last 30 million years. Because of the variable orbital forcing imprint recorded in the Site 1264 $CaCO_3$ content, we employed three distinct tuning strategies to achieve a 30 Myr astrochronology: I.a) 30-9.7 Ma: $CaCO_3$ content(/benthic $\delta^{18}O$) to eccentricity; I.b) 9.7-8.0 Ma: $CaCO_3$ content to E(T); II) 8.0-3.3 Ma: $CaCO_3$ content(/benthic $\delta^{18}O$) to ET-P; and III) 3.3-0.0 Ma: benthic $\delta^{18}O$ to LR04.

The $\%CaCO_3$ and $CaCO_3$ MARs were used to investigate carbonate deposition in the Southeastern Atlantic since the Oligocene. We recognise three distinct orbital pacings of the short-term $\%CaCO_3$ variability, broadly related to major changes in climate, the cryosphere and/or the carbon cycle: 1) ~110 kyr eccentricity-driven pacing dominates from 30 to ~13 Ma during Oligo-Miocene global warmth; 2) eccentricity-modulated precession-driven pacing appears after the mMCT and prevails from 14-8 Ma; 3) increased obliquity/precession-driven pacing prevails between ~7.7-3.3 Ma, following increased influence of high-latitude processes.

The lowest $CaCO_3$ content (92-94%) occurs between 18.5-14.4 Ma, suggesting increased dissolution and/or decreased carbonate rain at Site 1264, potentially caused by the widespread the global warmth associated with the MCO. However, the low $CaCO_3$ content at Site 1264 precede the MCO by ~1.5 Myr, in line with evidence for dissolution-induced $\%CaCO_3$ lows in the equatorial Pacific Ocean 1.0-0.5 Myr before the MCO. This may indicate that the global warmth and Antarctic deglaciation across the MCO was preconditioned for up to ~1.5 Myr by a prolonged interval of early Miocene global warmth. The emergence of precession-driving pacing in the Site 1264 $CaCO_3$ content after ~14 Ma suggests that Antarctic ice sheet expansion and global cooling across the MMCT caused regional productivity to become more sensitive to precession forcing and/or signifies the appearance of cooler, less corrosive deep-waters at Site 1264 better preserving precession-driven productivity cycles.

In association with the late Miocene Biogenic Bloom (LMBB), the highest $CaCO_3$ (95-97.5%) occur between ~8-4 Ma and the highest $CaCO_3$ MARs (~2-4.5 g/cm^2/kyr) are found between ~7.8-3.3 Ma. The onset of elevated $CaCO_3$ MARs (~7.8 Ma) roughly coincides with the shift from eccentricity-precession pacing to pervading obliquity-precession pacing of $\%CaCO_3$. The timing of the LMBB in the Site 1264 MARs agrees well with the onset in the eastern equatorial Pacific (EEP), although the LMBB lasts ~1 Myr longer in the South Atlantic (~3.3 Ma) than in the EEP (~4.4 Ma). Global patterns in the

https://doi.org/10.5194/cp-2020-108
Preprint. Discussion started: 4 September 2020

LMBB may be driven by increased nutrient input through increased late Miocene glacial weathering and/or increased weathering associated with Himalayan uplift/intensification of the monsoon. A global increase in the oceanic nutrient flux may be related to increased dust input following increased continental aridification and enhanced trade winds due to the increased latitudinal temperature gradients that appeared during the late Miocene cooling (7-5.4 Ma). Regional differences in the expression of the LMBB most likely reflect changes in oceanic nutrients distribution driven by regional differences in the extent of the late Miocene cooling, diachrony in the spread of continental aridification and/or changes in oceanic circulation following the late Miocene carbon isotope shift. Further work will be needed to disentangle global versus regional productivity patterns and explore causal links in greater detail.

Author Contributions and Competing Interests

AJD, DL, LL and TW designed the study. AJD, DL, TW, HB, NR, RW and ML contributed to the data collection and analysis. AJD, DL, TW and LL contributed to the stratigraphy and astrochronology. AJD wrote the manuscript with input from all co-authors. The authors declare that they have no conflict of interest.

Acknowledgements

This research used samples and data provided by the Ocean Drilling Program (ODP), sponsored by the US National Science Foundation (NSF) and participating countries. This research used data acquired at the XRF Core Scanner Lab at the MARUM – Center for Marine Environmental Sciences, University of Bremen, Germany. We especially thank Ursula Röhl and Vera Lukies (MARUM) for assistance with XRF core scanning and Alex Wülbers, Walter Hale and Holger Kuhlmann (IODP Bremen Core Repository) for core handling, and Tim van Peer for valuable discussions. Funding for this research was provided by the Deutsche Forschungsgemeinschaft (DFG, German Research Foundation) to TW and AJD (Project number 242225091, 408101468). AJD and DL were postdoctoral researchers and HP was the principal investigator in ERC Consolidator grant "EARTHSEQUENCING" (grant agreement 617462). AJD is currently funded by the European Union's Horizon 2020 research and innovation programme under the Marie Sklodowska-Curie grant agreement No 796220. ML was funded by NSF grant OCE-1656960.

Data availability

All data is archived on the open access database PANGAEA (https://doi.pangaea.de/10.1594/PANGAEA.919489). Further supplementary information is also available with the online version of this manuscript on the *Climate of the Past* website. A list of Supplemental Tables and Figures is provided here (tables marked with an * are also archived on PANGAEA):

https://doi.org/10.5194/cp-2020-108
Preprint. Discussion started: 4 September 2020


Climate of the Past Discussions

Supplementary tables:

1) Site 1264 XRF and Site 1264/1265 $CaCO_3$ data*
2) Offsets/affine tables for 1264*
3) Splice tie/interval tables for 1264*
4) Mapping tables for 1264*
5) 1264-1265 correlation to accommodate splice revisions*
6) Selected (i.e. high-quality) bio- and magnetostratigraphic events for Site 1264
7) New astrochronology for Site 1264*

Supplementary figures:

1) XRF intercalibration of the four measurement campaigns
2) Splice revision panels for entire interval showing revisions.
3) Revisions to the offsplice mapping pairs of Core 1264B-29H
4) Generation of the composite core image of ODP Sites 1264 and 1265.
5) Calibration of ln(Ca/Fe) to shipboard %$CaCO_3$
6) Calculation of bulk and $CaCO_3$ MARs
7) Polynomial fit through the selected (i.e. high-quality) bio- and magnetostratigraphic events for Site 1264
8) Spectral analysis of %$CaCO_3$ on the polynomial age model
9) Antiphase relationship between benthic $\delta^{18}O$ and %$CaCO_3$

References

Van Andel, T. H., Heath, G. R. and Moore, T. C.: Cenozoic History and Paleoceanography of the Central Equatorial Pacific Ocean, Mem. Geol. Soc. Am., 143, 1–223, doi:10.1130/MEM143-p1, 1975.

Badger, M. P. S., Lear, C. H., Pancost, R. D., Foster, G. L., Bailey, T. R., Leng, M. J. and Abels, H. A.: CO 2 drawdown following the middle Miocene expansion of the Antarctic Ice Sheet, , 28, 42–53, doi:10.1002/palo.20015, 2013.

Bailey, I., Hole, G. M., Foster, G. L., Wilson, P. A., Storey, C. D., Trueman, C. N. and Raymo, M. E.: An alternative suggestion for the Pliocene onset of major northern hemisphere glaciation based on the geochemical provenance of North Atlantic Ocean ice-rafted debris, Quat. Sci. Rev., 75, 181–194, doi:10.1016/j.quascirev.2013.06.004, 2013.

Barry, T. L., Kelley, S. P., Reidel, S. P., Camp, V. E., Self, S., Jarboe, N. A., Duncan, R. A. and Renne, P. R.: Eruption chronology of the Columbia River Basalt Group, Spec. Pap. Geol. Soc. Am., 497, 45–66, doi:10.1130/2013.2497(02), 2013.

Beddow, H. M., Liebrand, D., Sluijs, A., Wade, B. S. and Lourens, L. J.: Global change across the Oligocene-Miocene transition: High-resolution stable isotope records from IODP Site U1334 (equatorial Pacific Ocean), Paleoceanography, 31(1), 81–97, doi:10.1002/2015PA002820, 2016.

Beddow, H. M., Liebrand, D., Wilson, D. S., Hilgen, F. J., Sluijs, A., Wade, B. S. and Lourens, L. J.: Astronomical tunings of the Oligocene-Miocene transition from Pacific Ocean Site U1334 and implications for the carbon cycle, Clim. Past, 14(3), 255–270, doi:10.5194/cp-14-255-2018, 2018.

https://doi.org/10.5194/cp-2020-108
Preprint. Discussion started: 4 September 2020

Behrensmeyer, A. K., Quade, J., Cerling, T. E., Kappelman, J., Khan, I. A., Copeland, P., Roe, L., Hicks, J., Stubblefield, P., Willis, B. J. and Latorre, C.: The structure and rate of late Miocene expansion of C4 plants: Evidence from lateral variation in stable isotopes in paleosols of the Siwalik Group, northern Pakistan, Geol. Soc. Am. Bull., 119(11–12), 1486–1505, doi:10.1130/b26064.1, 2007.

Bell, D. B., Jung, S. J. A., Kroon, D., Lourens, L. L. and Hodell, D. A.: Local and regional trends in Plio-Pleistocene $\delta^{18}O$ records from benthic foraminifera, Geochemistry, Geophys. Geosystems, 3304–3321, doi:10.1002/2014GC005297.Received, 2014.

Bell, D. B., Jung, S. J. A., Kroon, D., Hodell, D. A., Lourens, L. J. and Raymo, M. E.: Atlantic Deep-water Response to the Early Pliocene Shoaling of the Central American Seaway., Sci. Rep., 5, 12252, doi:10.1038/srep12252, 2015.

Berger, W. H.: Biogenous Deep-Sea Sediments : Fractionation by Deep-Sea Circulation, , (May), 1970.

Billups, K. and Schrag, D. P. D. P.: Paleotemperatures and ice volume of the past 27 Myr revisited with paired Mg/Ca and 18O/16O measurements on benthic foraminifera, Paleoceanography, 17(1), doi:1003 10.1029/2000pa000567, 2002.

Bolton, C. T. and Stoll, H. M.: Late Miocene threshold response of marine algae to carbon dioxide limitation, Nature, 500(7464), 558–62, doi:10.1038/nature12448, 2013.

Cahoon, E. B., Streck, M. J., Koppers, A. A. P. and Miggins, D. P.: Reshuffling the Columbia river basalt chronology-picture gorge basalt, the earliest-and longest-erupting formation, Geology, 48(4), 348–352, doi:10.1130/G47122.1, 2020.

Carter, S. C., Griffith, E. M. and Penman, D. E.: Peak intervals of equatorial Pacific export production during the middle Miocene climate transition, Geology, 44(11), 923–926, doi:10.1130/G38290.1, 2016.

Cerling, T. E., Harris, J. M., MacFadden, B. J., Leakey, M. G., Quade, J., Eisenmann, V. and Ehleringer, J. R.: Global vegetation change through the Miocene/Pliocene boundary, Nature, 389(6647), 153–158, doi:10.1038/38229, 1997.

Connell, S. O., Wolf-Welling, T. C. W., Cremer, M., Stein, R. and O'Connell, S.: Neogene Paleoceanography and Paleoclimate history from Fram Strait: changes in accumulation rates, in Proceedings of the Ocean Drilling Program, Scientific Results, vol. 151, edited by J. Thiede, A. M. Myhre, J. V Firth, G. I. Johson, and W. F. Ruddiman, pp. 569–582., 1996.

Coxall, H. K. and Wilson, P. A.: Early Oligocene glaciation and productivity in the eastern equatorial Pacific: Insights into global carbon cycling, Paleoceanography, 26(2), 1–18, doi:10.1029/2010PA002021, 2011.

Dickens, G. R. and Owen, R. M.: The Latest Miocene-Early Pliocene biogenic bloom: A revised Indian Ocean perspective, Mar. Geol., 161(1), 75–91, doi:10.1016/S0025-3227(99)00057-2, 1999.

Diester-Haass, L., Meyers, P. A. and Vidal, L.: The late Miocene onset of high productivity in the Benguela Current upwelling system as part of a global pattern, Mar. Geol., 180(1–4), 87–103, doi:Pii S0025-3227(01)00207-9, 2002.

Diester-Haass, L., Meyers, P. A. and Bickert, T.: Carbonate crash and biogenic bloom in the late Miocene: Evidence from ODP Sites 1085, 1086, and 1087 in the Cape Basin, southeast Atlantic Ocean, Paleoceanography, 19(1), 1–19, doi:10.1029/2003PA000933, 2004.

Diester-Haass, L., Billups, K. and Emeis, K. C.: In search of the late Miocene-early Pliocene "biogenic bloom" in the Atlantic Ocean (Ocean Drilling Program Sites 982, 925, and 1088), Paleoceanography, 20(4), 1–13, doi:10.1029/2005PA001139, 2005.

Diester-Haass, L., Billups, K. and Emeis, K. C.: Late Miocene carbon isotope records and marine biological productivity: Was there a (dusty) link?, Paleoceanography, 21(4), 1–18, doi:Pa421610.1029/2006pa001267, 2006.

Drury, A. J., John, C. M. and Shevenell, A. E.: Evaluating climatic response to external radiative forcing during the late Miocene to early Pliocene: New perspectives from eastern equatorial Pacific (IODP U1338) and North Atlantic (ODP 982) locations, Paleoceanography, 31(1), 167–184, doi:10.1002/2015PA002881, 2016.

Drury, A. J., Westerhold, T., Frederichs, T., Tian, J., Wilkens, R., Channell, J. E. T., Evans, H., John, C. M., Lyle, M. and

https://doi.org/10.5194/cp-2020-108
Preprint. Discussion started: 4 September 2020

Röhl, U.: Late Miocene climate and time scale reconciliation: Accurate orbital calibration from a deep-sea perspective, Earth Planet. Sci. Lett., 475(C), 254–266, doi:10.1016/j.epsl.2017.07.038, 2017.

Drury, A. J., Lee, G. P., Gray, W. R., Lyle, M., Westerhold, T., Shevenell, A. E., John, C. M., C. M. John and John, C. M.: Deciphering the state of the late Miocene to early Pliocene equatorial Pacific, Paleoceanogr. Paleoclimatology, 33(3), 246–263, doi:10.1002/2017PA003245, 2018a.

Drury, A. J., Westerhold, T., Hodell, D. and Röhl, U.: Reinforcing the North Atlantic backbone: revision and extension of the composite splice at ODP Site 982, Clim. Past, 14(3), 321–338, doi:10.5194/cp-14-321-2018, 2018b.

Dupont, L. M., Rommerskirchen, F., Mollenhauer, G. and Schefuß, E.: Miocene to Pliocene changes in South African hydrology and vegetation in relation to the expansion of C4 plants, Earth Planet. Sci. Lett., 375, 408–417, doi:10.1016/j.epsl.2013.06.005, 2013.

Farrell, J., Raffi, I. and Janecek, T.: Late Neogene sedimentation patterns in the eastern equatorial Pacific Ocean, Proc. ODP, Sci. Results, 138, 717–756 [online] Available from: http://cat.inist.fr/?aModele=afficheN&cpsidt=3010133 (Accessed 5 April 2014), 1995.

Filippelli, G. M.: Intensification of the Asian monsoon and a chemical weathering event in the late Miocene-early Pliocene: Implications for late Neogene climate change, Geology, 25(1), 27–30, doi:10.1130/0091-7613(1997)025<0027, 1997.

Foster, G. L., Lear, C. H. and Rae, J. W. B.: The evolution of pCO2 , ice volume and climate during the middle Miocene, Earth Planet. Sci. Lett., 341–344, 243–254, 2012.

Fronval, T. and Jansen, E.: Late Neogene paleoclimates and paleoceanography in the Iceland-Norwegian Sea: evidence from the Iceland and Vøring Plateaus, Proc. ODP, 151(1988), 455–468, doi:10.2973/odp.proc.sr.151.134.1996, 1996.

Gasson, E., Deconto, R. M., Pollard, D. and Levy, R. H.: Dynamic Antarctic ice sheet during the early to mid-Miocene, Proc. Natl. Acad. Sci. U. S. A., 113(13), 3459–3464, doi:10.1073/pnas.1516130113, 2016.

Grant, K. M. and Dickens, G. R.: Coupled productivity and carbon isotope records in the southwest Pacific Ocean during the late Miocene-early Pliocene biogenic bloom, Palaeogeogr. Palaeoclimatol. Palaeoecol., 187(1–2), 61–82, doi:10.1016/S0031-0182(02)00508-4, 2002.

Greenop, R., Foster, G. L., Wilson, P. A. and Lear, C. H.: Middle Miocene climate instability associated with high-amplitude CO<inf>2</inf> variability, Paleoceanography, 29(9), 845–853, doi:10.1002/2014PA002653, 2014.

Grinsted, A., Moore, J. C. and Jevrejeva, S.: Application of the cross wavelet transform and wavelet coherence to geophysical time series, Nonlinear Process. Geophys., 11(5/6), 561–566, doi:10.5194/npg-11-561-2004, 2004.

Haq, B., Worsley, T. and Burckle, L.: Late Miocene marine carbon-isotopic shift and synchroneity of some phytoplanktonic biostratigraphic events, Geology, 8, 427–431 [online] Available from: http://geology.gsapubs.org/content/8/9/427.short (Accessed 5 April 2014), 1980.

Herbert, T. D., Lawrence, K. T., Tzanova, A., Peterson, L. C., Caballero-Gill, R. and Kelly, C. S.: Late Miocene global cooling and the rise of modern ecosystems, Nat. Geosci, advance on(11), 843–847, doi:10.1038/ngeo2813, 2016.

Hermoyian, C. S. and Owen, R. M.: Late miocene-early pliocene biogenic bloom: Evidence from low-productivity regions of the Indian and Atlantic Oceans, Paleoceanography, 16(1), 95–100, doi:10.1029/2000pa000501, 2001.

Hodell, D. A. and Venz-Curtis, K. A.: Late Neogene history of deepwater ventilation in the Southern Ocean, Geochemistry Geophys. Geosystems, 7(9), (Q09001), doi:10.1029/2005GC001211, 2006.

Hodell, D. A., Curtis, J. H., Sierro, F. J. and Raymo, M. E.: Correlation of late Miocene to early Pliocene sequences between the Mediterranean and North Atlantic, Paleoceanography, 16(2), 164–178, doi:10.1029/1999pa000487, 2001.

Holbourn, A., Kuhnt, W., Schulz, M. and Erlenkeuser, H.: Impacts of orbital forcing and atmospheric carbon dioxide on Miocene ice-sheet expansion, Nature, 438(7067), 483–487, doi:10.1038/nature04123, 2005.

https://doi.org/10.5194/cp-2020-108
Preprint. Discussion started: 4 September 2020

Holbourn, A., Kuhnt, W., Lyle, M., Schneider, L., Romero, O. and Andersen, N.: Middle Miocene climate cooling linked to intensification of eastern equatorial Pacific upwelling, Geology, 42(1), 19–22, doi:10.1017/CBO9781107415324.004, 2014.

Holbourn, A., Kuhnt, W., Kochhann, K. G. D., Andersen, N. and Sebastian Meier, K. J.: Global perturbation of the carbon cycle at the onset of the Miocene Climatic Optimum, Geology, 43(2), 123–126, doi:10.1130/G36317.1, 2015.

Holbourn, A. E., Kuhnt, W., Clemens, S. C., Kochhann, K. G. D. D., Jöhnck, J., Lübbers, J. and Andersen, N.: Late Miocene climate cooling and intensification of southeast Asian winter monsoon, Nat. Commun., 9(1), 1584, doi:10.1038/s41467-018-03950-1, 2018.

Hovan, S. A.: Late Cenozoic Atmospheric Circulation Intensity and Climatic History Recorded by Eolian Deposition in the Eastern Equatorial Pacific Ocean, Leg 138, Proc. Ocean Drill. Program, 138 Sci. Results, 138, doi:10.2973/odp.proc.sr.138.132.1995, 1995.

John, C. M., Karner, G. D., Browning, E., Leckie, R. M., Mateo, Z., Carson, B. and Lowery, C.: Timing and magnitude of Miocene eustasy derived from the mixed siliciclastic-carbonate stratigraphic record of the northeastern Australian margin, Earth Planet. Sci. Lett., 304(3–4), 455–467, doi:10.1016/j.epsl.2011.02.013, 2011.

Kasbohm, J. and Schoene, B.: Rapid eruption of the Columbia River flood basalt and correlation with the mid-Miocene climate optimum, Sci. Adv., 4(9), 1–9, doi:10.1126/sciadv.aat8223, 2018.

Keating-Bitonti, C. R. and Peters, S. E.: Influence of increasing carbonate saturation in Atlantic bottom water during the late Miocene, Palaeogeogr. Palaeoclimatol. Palaeoecol., 518(January), 134–142, doi:10.1016/j.palaeo.2019.01.006, 2019.

Kochhann, K. G. D., Holbourn, A., Kuhnt, W., Channell, J. E. T., Lyle, M., Shackford, J. K., Wilkens, R. H. and Andersen, N.: Eccentricity pacing of eastern equatorial Pacific carbonate dissolution cycles during the Miocene Climatic Optimum, Paleoceanography, 31(9), 1176–1192, doi:10.1002/2016PA002988, 2016.

Kong, P., Huang, F., Liu, X., Fink, D., Ding, L. and Lai, Q.: Late Miocene ice sheet elevation in the Grove Mountains, East Antarctica, inferred from cosmogenic 21Ne–10Be–26Al, Glob. Planet. Change, 72(1–2), 50–54, doi:10.1016/j.gloplacha.2010.03.005, 2010.

Kroon, D., Steens, T. and Troelstra, S. R.: Onset of monsoonal related upwelling in the western Arabian Sea as revealed by planktonic foraminifers, Proc., Sci. results, ODP, Leg 117, Oman Margin/Neogene Packag., doi:10.2973/odp.proc.sr.117.126.1991, 1991.

Laskar, J., Robutel, P., Joutel, F., Gastineau, M., Correia, a. C. M. M. and Levrard, B.: A long-term numerical solution for the insolation quantities of the Earth, Astron. Astrophys., 428(1), 261–285, doi:10.1051/0004-6361:20041335, 2004.

Laskar, J., Gastineau, M., Delisle, J.-B., Farrés, a. and Fienga, a.: Strong chaos induced by close encounters with Ceres and Vesta, Astron. Astrophys., 532(2011), L4, doi:10.1051/0004-6361/201117504, 2011.

Lear, C. H., Elderfield, H. and Wilson, P. A.: Cenozoic deep-sea temperatures and global ice volumes from Mg/Ca in benthic foraminiferal calcite, Science (80-.)., 287(5451), 269–272, doi:10.1126/science.287.5451.269, 2000.

Lear, C. H., Coxall, H. K., Foster, G. L., Lunt, D. J., Mawbey, E. M., Rosenthal, Y., Sosdian, S. M., Thomas, E. and Wilson, P. A.: Neogene ice volume and ocean temperatures: Insights from infaunal foraminiferal Mg/Ca paleothermometry, Paleoceanography, n/a-n/a, doi:10.1002/2015PA002833, 2015.

Levy, R., Harwood, D. M., Florindo, F., Sangiorgi, F., Tripati, R., Eynatten, H. Von, von Eynatten, H., Gasson, E., Kuhn, G., Tripati, A., DeConto, R., Fielding, C., Field, B., Golledge, N., McKay, R., Naish, T., Olney, M. M., Pollard, D., Schouten, S., Talarico, F., Warny, S., Willmott, V., Acton, G., Panter, K., Paulsen, T., Taviani, M., Askin, R., Atkins, C., Bassett, K., Beu, A., Blackstone, B., Browne, G., Ceregato, A., Cody, R., Cornamusini, G., Corrado, S., Del Carlo, P., Di Vincenzo, G., Dunbar, G., Falk, C., Frank, T., Giorgetti, G., Grelle, T., Gui, Z., Handwerger, D., Hannah, M., Harwood, D. M., Hauptvogel, D., Hayden, T., Henrys, S., Hoffmann, S., Iacoviello, F., Ishman, S., Jarrard, R., Johnson, K., Jovane, L., Judge, S., Kominz, M., Konfirst, M., Krissek, L., Lacy, L., Maffioli, P., Magens, D., Marcano, M. C., Millan, C., Mohr, B., Montone, P., Mukasa, S., Niessen, F., Ohneiser, C., Passchier, S., Patterson, M., Pekar, S., Pierdominici, S., Raine, I., Reed,

https://doi.org/10.5194/cp-2020-108
Preprint. Discussion started: 4 September 2020

J., Reichelt, L., Riesselman, C., Rocchi, S., Sagnotti, L., Sandroni, S., Schmitt, D., Speece, M., Storey, B., Strada, E., Tuzzi, E., Verosub, K., Wilson, G., Wilson, T., Wonik, T. and Zattin, M.: Antarctic ice sheet sensitivity to atmospheric CO2 variations in the early to mid-Miocene, Proc. Natl. Acad. Sci. U. S. A., 113(13), 3453–3458, doi:10.1073/pnas.1516030113, 2016.

Liao, Y. and Lyle, M.: Late Miocene to Pleistocene sedimentation and sediment transport on the Cocos Ridge, eastern tropical Pacific Ocean, Mar. Geol., 355, 1–14, doi:10.1016/j.margeo.2014.05.007, 2014.

Liebrand, D., Lourens, L. J., Hodell, D. A., de Boer, B., Van De Wal, R. S. W. and Pälike, H.: Antarctic ice sheet and oceanographic response to eccentricity forcing during the early Miocene, Clim. Past, 7(3), 869–880, doi:10.5194/cp-7-869-2011, 2011.

Liebrand, D., Beddow, H. M., Lourens, L. J., Pälike, H., Raffi, I., Bohaty, S. M., Hilgen, F. J., Saes, M. J. M. M., Wilson, P. A., van Dijk, A. E., Hodell, D. A., Kroon, D., Huck, C. E., Batenburg, S. J., Dijk, A. E. Van, Hodell, D. A., Kroon, D., Huck, C. E. and Batenburg, S. J.: Cyclostratigraphy and eccentricity tuning of the early Oligocene through early Miocene (30.1–17.1 Ma): Cibicides mundulus stable oxygen and carbon isotope records from Walvis Ridge Site 1264, Earth Planet. Sci. Lett., 1, 1–14, doi:10.1016/j.epsl.2016.06.007, 2016.

Liebrand, D., de Bakker, A. T. M., Beddow, H. M., Wilson, P. A., Bohaty, S. M., Ruessink, G., Pälike, H., Batenburg, S. J., Hilgen, F. J., Hodell, D. A., Huck, C. E., Kroon, D., Raffi, I., Saes, M. J. M., van Dijk, A. E. and Lourens, L. J.: Evolution of the early Antarctic ice ages, Proc. Natl. Acad. Sci., 114(15), 3867–3872, doi:10.1073/pnas.1615440114, 2017.

Liebrand, D., Raffi, I., Fraguas, Á., Laxenaire, R., Bosmans, J. H. C., Hilgen, F. J., Wilson, P. A., Batenburg, S. J., Beddow, H. M., Bohaty, S. M., Bown, P. R., Crocker, A. J., Huck, C. E., Lourens, L. J. and Sabia, L.: Orbitally Forced Hyperstratification of the Oligocene South Atlantic Ocean, Paleoceanogr. Paleoclimatology, 33(5), 511–529, doi:10.1002/2017PA003222, 2018.

Lisiecki, L. E. and Raymo, M. E.: A Pliocene-Pleistocene stack of 57 globally distributed benthic $\delta^{18}O$ records, Paleoceanography, 20(1), PA1003, doi:10.1029/2004PA001071, 2005.

Littler, K., Westerhold, T., Drury, A. J., Liebrand, D., Lisiecki, L. and Pälike, H.: Astronomical time keeping of earth history: An invaluable contribution of scientific ocean drilling, Oceanography, 32(1), 72–76, doi:10.5670/oceanog.2019.122, 2019.

Lourens, L., Hilgen, F. J., Shackleton, N. J., Laskar, J. and Wilson, D.: The Neogene Period, in A Geologic Time Scale 2004, edited by F. M. Gradstein, J. G. Ogg, and A. G. Smith, pp. 409–440, Cambridge University Press., 2004.

Lyle, M.: Neogene carbonate burial in the Pacific Ocean, Paleoceanography, 18(3), 1–19, doi:10.1029/2002PA000777, 2003.

Lyle, M. and Baldauf, J.: Biogenic sediment regimes in the Neogene equatorial Pacific, IODP Site U1338: Burial, production, and diatom community, Palaeogeogr. Palaeoclimatol. Palaeoecol., 433, 106–128, doi:10.1016/j.palaeo.2015.04.001, 2015.

Lyle, M., Dadey, K. A. K. a K. A. K. A. and Farrell, J. W. J. W. J. W. J. W.: The late Miocene (11–8 Ma) eastern Pacific carbonate crash: evidence for reorganization of deep-water circulation by the closure of the Panama Gateway. , edited by N. G. Pisias Mayer, L.A., Janecek, T.R., Palmer-Julson, A., van Andel, T.H., Proc. ODP, Sci. Results, 138, 821–838, doi:10.2973/odp.proc.sr.138.157.1995, 1995.

Lyle, M., Barron, J., Bralower, T. J., Huber, M., Lyle, A. O., Ravelo, A. C., Rea, D. K. and Wilson, P. A.: Pacific ocean and Cenozoic evolution of climate, Rev. Geophys., 46(2), doi:Rg2002 10.1029/2005rg000190, 2008.

Lyle, M., Drury, A. J., Tian, J., Wilkens, R. and Westerhold, T.: Late Miocene to Recent High Resolution Eastern Equatorial Pacific Carbonate Records: Stratigraphy linked by dissolution and paleoproductivity, Clim. Past Discuss., 15(December), 1–41, doi:10.5194/cp-2018-157, 2019.

Mejía, L. M., Méndez-Vicente, A., Abrevaya, L., Lawrence, K. T., Ladlow, C., Bolton, C., Cacho, I. and Stoll, H.: A diatom

https://doi.org/10.5194/cp-2020-108
Preprint. Discussion started: 4 September 2020

record of CO_2 decline since the late Miocene, Earth Planet. Sci. Lett., 479, 18–33, doi:10.1016/j.epsl.2017.08.034, 2017.

Miller, K. G., Wright, J. D. and Fairbanks, R. G.: Unlocking the ice house: Oligocene-Miocene oxygen isotopes, eustasy, and margin erosion, J. Geophys. …, 96(B4), 6829–6848 [online] Available from: http://onlinelibrary.wiley.com/doi/10.1029/90JB02015/full (Accessed 5 April 2014), 1991.

Molnar, P.: Mio-pliocene growth of the Tibetan plateau and evolution of East Asian climate, Palaeontol. Electron., 8(1), 1–23, 2005.

Moore, N. E., Grunder, A. L. and Bohrson, W. A.: The three-stage petrochemical evolution of the Steens Basalt (southeast Oregon, USA) compared to large igneous provinces and layered mafic intrusions, Geosphere, 14(6), 2505–2532, doi:10.1130/GES01665.1, 2018.

Moore, N. E., Grunder, A. L., Bohrson, W. A., Carlson, R. W. and Bindeman, I. N.: Changing mantle sources and the effects of crustal passage on the Steens Basalt, SE Oregon: Chemical and isotopic constraints, Geochemistry, Geophys. Geosystems, 1–33, doi:10.1029/2020gc008910, 2020.

Ohneiser, C. and Wilson, G. S.: Eccentricity-Paced Southern Hemisphere Glacial-Interglacial Cyclicity Preceding the Middle Miocene Climatic Transition, Paleoceanogr. Paleoclimatology, 33(7), 795–806, doi:10.1029/2017PA003278, 2018.

Pälike, H., Norris, R. D., Herrle, J. O., Wilson, P. A., Coxall, H. K., Lear, C. H., Shackleton, N. J., Tripati, A. K. and Wade, B. S.: The heartbeat of the Oligocene climate system., Science, 314(5807), 1894–8, doi:10.1126/science.1133822, 2006.

Pälike, H., Lyle, M. W., Nishi, H., Raffi, I., Ridgwell, A., Gamage, K., Klaus, A., Acton, G., Anderson, L., Backman, J., Baldauf, J., Beltran, C., Bohaty, S. M., Bown, P., Busch, W., Channell, J. E. T. T., Chun, C. O. J. J., Delaney, M., Dewangan, P., Dunkley Jones, T., Edgar, K. M., Evans, H., Fitch, P., Foster, G. L., Gussone, N., Hasegawa, H., Hathorne, E. C., Hayashi, H., Herrle, J. O., Holbourn, A., Hovan, S., Hyeong, K., Iijima, K., Ito, T., Kamikuri, S. I., Kimoto, K., Kuroda, J., Leon-Rodriguez, L., Malinverno, A., Moore, T. C., Murphy, B. H., Murphy, D. P., Nakamura, H., Ogane, K., Ohneiser, C., Richter, C., Robinson, R., Rohling, E. J., Romero, O., Sawada, K., Scher, H., Schneider, L., Sluijs, A., Takata, H., Tian, J., Tsujimoto, A., Wade, B. S., Westerhold, T., Wilkens, R., Williams, T., Wilson, P. a., Yamamoto, Y., Yamamoto, S., Yamazaki, T., Zeebe, R. E., Palike, H., Jones, T. D., Moore, Ted, C., Murphy, B. H., Murphy, D. P., Nakamura, H., Ogane, K., Ohneiser, C., Richter, C., Robinson, R., Rohling, E. J., Romero, O., Sawada, K., Scher, H., Schneider, L., Sluijs, A., Takata, H., Tian, J., Tsujimoto, A., Wade, B. S., Westerhold, T., Wilkens, R., Williams, T., Wilson, P. a., Yamamoto, Y., Yamamoto, S., Yamazaki, T., Zeebe, R. E., Moore, T. C., Murphy, B. H., Murphy, D. P., Nakamura, H., Ogane, K., et al.: A Cenozoic record of the equatorial Pacific carbonate compensation depth, Nature, 488(7413), 609–614, doi:10.1038/nature11360, 2012.

Piela, C., Lyle, M., Marcantonio, F., Baldauf, J. and Olivarez Lyle, A.: Biogenic sedimentation in the equatorial Pacific: Carbon cycling and paleoproduction, 12-24 Ma, Paleoceanography, 27(2), 12–24, doi:10.1029/2011PA002236, 2012.

Pound, M. J., Haywood, A. M., Salzmann, U., Riding, J. B., Lunt, D. J. and Hunter, S. J.: A Tortonian (Late Miocene, 11.61-7.25 Ma) global vegetation reconstruction, Palaeogeogr. Palaeoclimatol. Palaeoecol., 300(1–4), 29–45, doi:10.1016/j.palaeo.2010.11.029, 2011.

Pound, M. J., Haywood, A. M., Salzmann, U. and Riding, J. B.: Global vegetation dynamics and latitudinal temperature gradients during the Mid to Late Miocene (15.97-5.33 Ma), Earth-Science Rev., 112(1–2), 1–22, doi:10.1016/j.earscirev.2012.02.005, 2012.

Reghellin, D., Coxall, H. K., Dickens, G. R. and Backman, J.: Carbon and oxygen isotopes of bulk carbonate in sediment deposited beneath the eastern equatorial Pacific over the last 8 million years, Paleoceanography, 30(10), 1261–1286, doi:10.1002/2015PA002825, 2015.

Reghellin, D., Dickens, G. R., Coxall, H. K. and Backman, J.: Understanding Bulk Sediment Stable Isotope Records in the Eastern Equatorial Pacific, From Seven Million Years Ago to Present Day, Paleoceanogr. Paleoclimatology, 35(2), 1–22, doi:10.1029/2019PA003586, 2020.

Schuster, M., Duringer, P., Ghienne, J. F., Vignaud, P., Mackaye, H. T., Likius, A. and Brunet, M.: The age of the Sahara

desert, Science (80-.)., doi:10.1126/science.1120161, 2006.

Seidov, D. A. N. and Maslin, M.: Atlantic Ocean heat piracy and the bipolar climate see-saw during Heinrich and Dansgaard – Oeschger events, , 16, 321–328, doi:10.1002/jqs.595, 2001.

Shackleton, N. J. and Hall, M. A.: The Late Miocene Stable Isotope Record, Site 926, in Proceedings of the Ocean Drilling Program, Scientific Results, vol. 154, edited by N. J. Shackleton, W. B. Curry, C. Richter, and T. J. Bralower, pp. 367–373, College Station, TX (Ocean Drilling Program)., 1997.

Shackleton, N. J., Hall, M. A. and Pate, D.: Pliocene Stable Isotope Stratigraphy of Site 846, edited by N. G. Pisias, L. A. Mayer, T. R. Janecek, A. Palmer-Julson, and T. H. van Andel, Proc. ODP, Sci. Results, 138, 337–355, 1996.

Shevenell, A. E., Kennett, J. P. and Lea, D. W.: Middle Miocene Southern Ocean Cooling and Antarctic Cryosphere Expansion, Science (80-.)., 305(5691), 1766–1770, doi:10.1126/science.1100061, 2004.

Shevenell, A. E., Kennett, J. P. and Lea, D. W.: Middle Miocene ice sheet dynamics, deep-sea temperatures, and carbon cycling: A Southern Ocean perspective, Geochemistry, Geophys. Geosystems, 9(2), doi:10.1029/2007gc001736, 2008.

Shipboard Scientific Party Leg 208: Site 1264, in Proceedings of the Ocean Drilling Program, Initial Reports, vol. 208, edited by J. C. Zachos, D. Kroon, P. Blum, and Shipboard Scientific Party Leg 208, pp. 1–87, College Station, TX (Ocean Drilling Program)., 2004a.

Shipboard Scientific Party Leg 208: Site 1265, in Proceedings of the Ocean Drilling Program, Initial Reports, vol. 208, edited by J. C. Zachos, D. Kroon, P. Blum, and Shipboard Scientific Party Leg 208, pp. 1–87, College Station, TX (Ocean Drilling Program)., 2004b.

Shipboard Scientific Party Leg 208: Site 1267, in Proceedings of the Ocean Drilling Program, Initial Reports, vol. 208, edited by J. C. Zachos, D. Kroon, P. Blum, and Shipboard Scientific Party Leg 208, pp. 1–87, College Station, TX (Ocean Drilling Program)., 2004c.

Sosdian, S. M., Babila, T. L., Greenop, R., Foster, G. L. and Lear, C. H.: Ocean Carbon Storage across the middle Miocene: a new interpretation for the Monterey Event, Nat. Commun., 11(1), 1–11, doi:10.1038/s41467-019-13792-0, 2020.

Super, J. R., Thomas, E., Pagani, M., Huber, M., Brien, C. O. and Hull, P. M.: North Atlantic temperature and pCO2 coupling in the early-middle Miocene, , 46(6), 519–522, doi:https://doi.org/10.1130/G40228.1, 2018.

Super, J. R., Thomas, E., Pagani, M., Huber, M., O'Brien, C. L. and Hull, P. M.: Miocene Evolution of North Atlantic Sea Surface Temperature, Paleoceanogr. Paleoclimatology, (November), e2019PA003748, doi:10.1029/2019pa003748, 2020.

Sutherland, R., Dickens, G. R., Blum, P., Agnini, C., Alegret, L., Asatryan, G., Bhattacharya, J., Bordenave, A., Chang, L., Collot, J., Cramwinckel, M. J., Dallanave, E., Drake, M. K., Etienne, S. J. G., Giorgioni, M., Gurnis, M., Harper, D. T., Huang, H.-H. M., Keller, A. L., Lam, A. R., Li, H., Matsui, H., Morgans, H. E. G., Newsam, C., Park, Y.-H., Pascher, K. M., Pekar, S. F., Penman, D. E., Saito, S., Stratford, W. R., Westerhold, T. and Zhou, X.: Expedition 371 summary., 2019.

Tauxe, L. and Feakins, S. J.: A re-assessment of the chronostratigraphy of late Miocene C 3 -C 4 transitions, , 1–26, doi:10.1029/2020PA003857, 2020.

Tian, J., Yang, M., Lyle, M. W., Wilkens, R. and Shackford, J. K.: Obliquity and long eccentricity pacing of the Middle Miocene climate transition, Geochemistry, Geophys. Geosystems, 14(6), 1740–1755, doi:10.1002/ggge.20108, 2013.

Tian, J., Ma, W., Lyle, M. W. and Shackford, J. K.: Synchronous mid-Miocene upper and deep oceanic $\delta^{13}C$ changes in the east equatorial Pacific linked to ocean cooling and ice sheet expansion, Earth Planet. Sci. Lett., 406(March), 72–80, doi:10.1016/j.epsl.2014.09.013, 2014.

Tian, J., Ma, X., Zhou, J., Jiang, X., Lyle, M., Shackford, J. and Wilkens, R.: Paleoceanography of the east equatorial Pacific over the past 16 Myr and Pacific–Atlantic comparison: High resolution benthic foraminiferal δ18O and δ13C records at IODP Site U1337, Earth Planet. Sci. Lett., 499, 185–196, doi:10.1016/j.epsl.2018.07.025, 2018.

Tipple, B. J. and Pagani, M.: The Early Origins of Terrestrial C4 Photosynthesis, Annu. Rev. Earth Planet. Sci., 35(1), 435–

461, doi:10.1146/annurev.earth.35.031306.140150, 2007.

Torrence, C. and Compo, G. P. G. P.: A practical guide to wavelet analysis, Bull. Am. Meteorol. Soc., 79(1), 61–78, doi:10.1175/1520-0477(1998)079<0061:APGTWA>2.0.CO;2, 1998.

Turner, S. K.: Pliocene switch in orbital-scale carbon cycle/climate dynamics, , (Figure 1), 1256–1266, doi:10.1002/2014PA002651.Received, 2014.

Uno, K. T., Polissar, P. J., Jackson, K. E. and deMenocal, P. B.: Neogene biomarker record of vegetation change in eastern Africa, Proc. Natl. Acad. Sci., 113(23), 6355–6363, doi:10.1073/pnas.1521267113, 2016.

De Vleeschouwer, D., Vahlenkamp, M., Crucifix, M. and Pälike, H.: Alternating Southern and Northern Hemisphere climate response to astronomical forcing during the past 35 m.y, Geology, 45(4), 375–378, doi:10.1130/G38663.1, 2017.

Voigt, J., Hathorne, E. C., Frank, M. and Holbourn, A.: Minimal influence of recrystallization on middle Miocene benthic foraminiferal stable isotope stratigraphy in the eastern equatorial Pacific, Paleoceanography, 31(1), 98–114, doi:10.1002/2015PA002822, 2016.

Wade, B. S.: Oligocene climate dynamics, , 19, 1–16, doi:10.1029/2004PA001042, 2004.

Westerhold, T., Röhl, U., Frederichs, T., Agnini, C., Raffi, I., Zachos, J. C. and Wilkens, R. H.: Astronomical calibration of the Ypresian timescale: Implications for seafloor spreading rates and the chaotic behavior of the solar system?, Clim. Past, 13(9), 1129–1152, doi:10.5194/cp-13-1129-2017, 2017.

Wilkens, R. H., Westerhold, T., Drury, A. J., Lyle, M., Gorgas, T. and Tian, J.: Revisiting the Ceara Rise, equatorial Atlantic Ocean: isotope stratigraphy of ODP Leg 154 from 0 to 5 Ma, Clim. Past, 13(7), 779–793, doi:https://doi.org/10.5194/cp-13-779-2017, 2017.

Williams, T., van de Flierdt, T., Hemming, S. R., Chung, E., Roy, M. and Goldstein, S. L.: Evidence for iceberg armadas from East Antarctica in the Southern Ocean during the late Miocene and early Pliocene, Earth Planet. Sci. Lett., 290(3–4), 351–361, doi:10.1016/j.epsl.2009.12.031, 2010.

Wolf-Welling, T. C. W., Cremer, M. M., Connell, S. O., Winkler, A., Thiede, J., O'Connell, S., Winkler, A. and Jörn, T.: Cenozoic Arctic Gateway paleoclimate variability: indications from changes in coarse-fraction composition, Proc. ODP, Sci. Results, 151, 515–567 [online] Available from: http://cat.inist.fr/?aModele=afficheN&cpsidt=2673720, 1996.

Yang, R., Yang, Y., Fang, X., Ruan, X., Galy, A., Ye, C., Meng, Q. and Han, W.: Late Miocene Intensified Tectonic Uplift and Climatic Aridification on the Northeastern Tibetan Plateau: Evidence From Clay Mineralogical and Geochemical Records in the Xining Basin, Geochemistry, Geophys. Geosystems, 20(2), 829–851, doi:10.1029/2018GC007917, 2019.

Zachos, J., Pagani, H., Sloan, L., Thomas, E. and Billups, K.: Trends, rhythms, and aberrations in global climate 65 Ma to present, Science (80-.)., 292(5517), 686–693, doi:10.1126/science.1059412, 2001.

Zeeden, C., Hilgen, F., Westerhold, T., Lourens, L., Röhl, U. and Bickert, T.: Revised Miocene splice, astronomical tuning and calcareous plankton biochronology of ODP Site 926 between 5 and 14.4Ma, Palaeogeogr. Palaeoclimatol. Palaeoecol., 369(August 2015), 430–451, doi:10.1016/j.palaeo.2012.11.009, 2013.

Zeeden, C., Hilgen, F. J., Hüsing, S. K. and Lourens, L. L.: The Miocene astronomical time scale 9-12-Ma: New constraints on tidal dissipation and their implications for paleoclimatic investigations, Paleoceanography, 29(4), 296–307, doi:10.1002/2014PA002615, 2014.

Zhisheng, A., Kutzbach, J. E., Prell, W. L. and Porter, S. C.: Evolution of Asian monsoons and phased uplift of the Himalaya-Tibetan plateau since Late Miocene times., Nature, 411(6833), 62–66, doi:10.1038/35075035, 2001.

https://doi.org/10.5194/cp-2020-108
Preprint. Discussion started: 4 September 2020

Climate of the Past Discussions
Open Access
EGU

Figure 1: (A) Site Overview showing location of Site 1264 and Site 1265 on the Angola Basin side of Walvis Ridge, as well as (B) the differences between core box photos and line-scan images compiled with CODD.

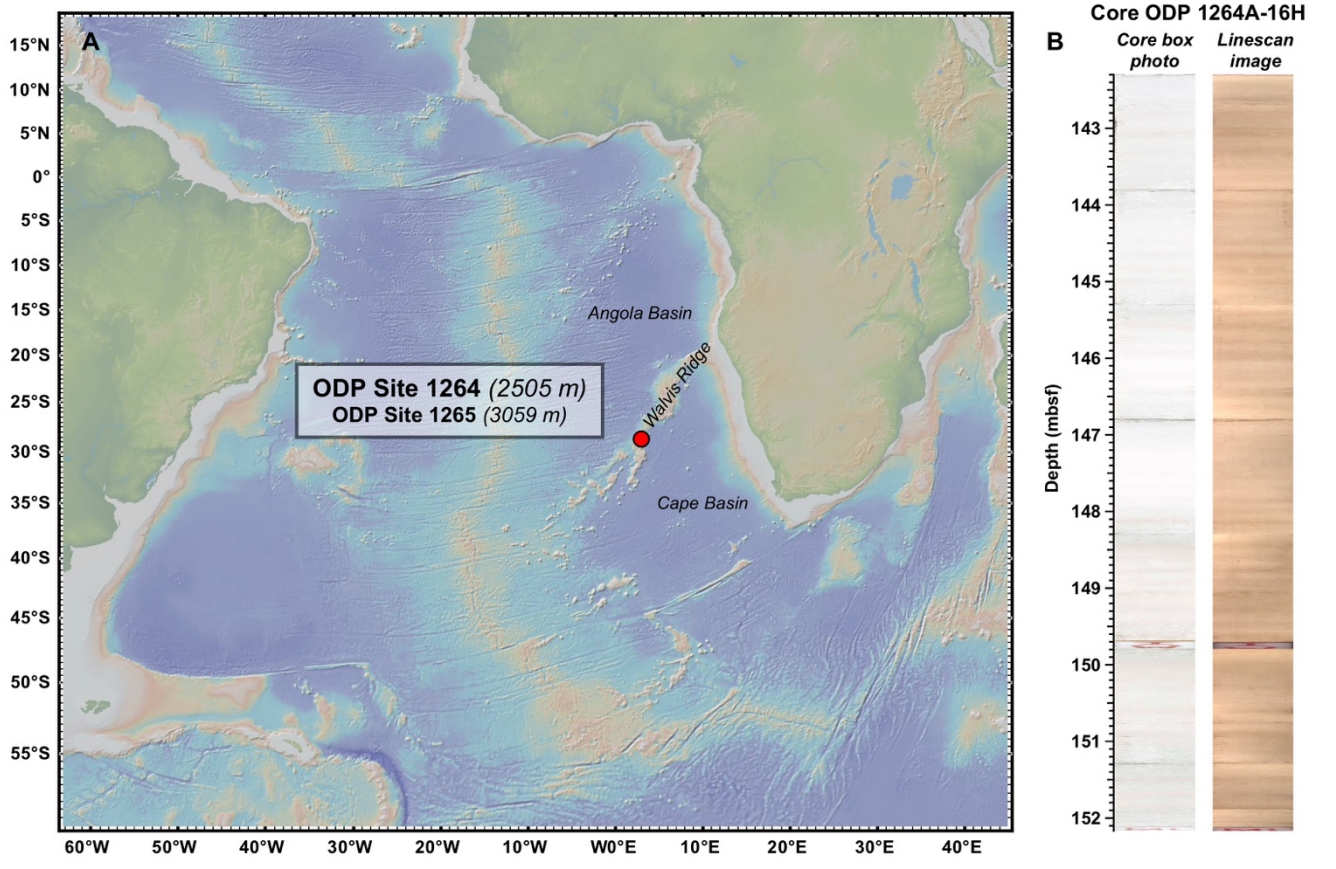

5

https://doi.org/10.5194/cp-2020-108
Preprint. Discussion started: 4 September 2020

Climate of the Past Discussions

Figure 2: Overview of main splice change between the shipboard splice (A) and the revised splice presented in this study (B). The interval between arrows on the splice was revised based on the ln(Ca/Fe) data. The shipboard MS is too low amplitude in the late Miocene in particular to robustly revise the splice, whereas ln(Ca/Fe) data showed the sedimentary variability well. In certain high $CaCO_3$ intervals Ba counts were also used to revise the composite splice (Supplementary Figure 2). The individual holes are shown for the shipboard splice only, with splice intervals shown between consecutive turquoise (top) and purple (bottom) vertical lines.

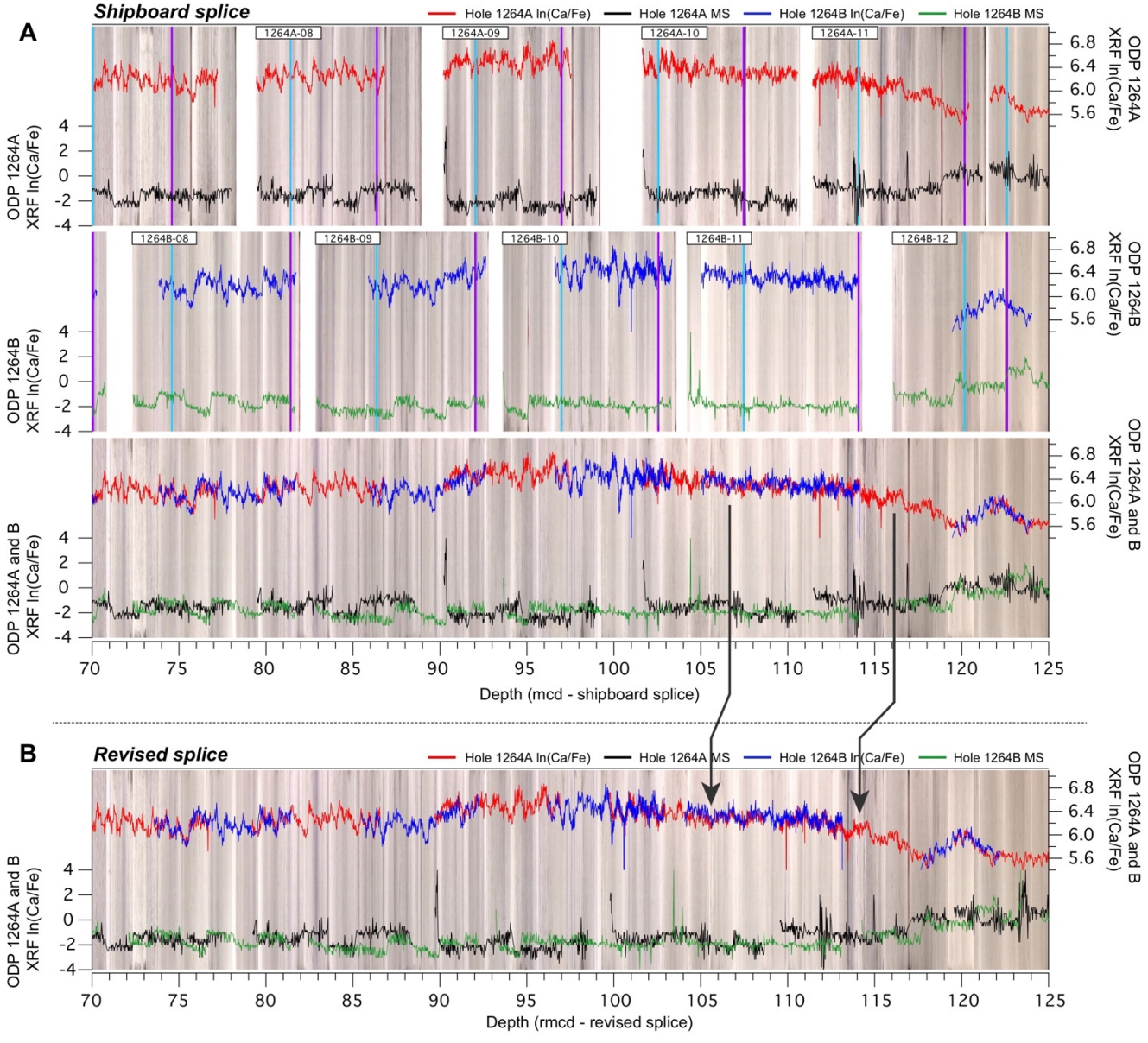

https://doi.org/10.5194/cp-2020-108
Preprint. Discussion started: 4 September 2020

Climate of the Past Discussions

Figure 3: On the new revised composite depth (rmcd) (A) Site 1264 XRF Si intensity (green), (B) %$CaCO_3$ data derived from ln(Ca/Fe) for Sites 1264 (dark red) and 1265 (black), (C) bulk and $CaCO_3$ MARs for Sites 1264 (dark and light blue, respectively) and 1265 (black and grey, respectively), (D) sedimentation rates in cm/kyr for Sites 1264 (grey) and 1265 (black), and the combined composite core photo for Sites 1264 and 1265 compiled using line scan (E) and core box photo images (F).

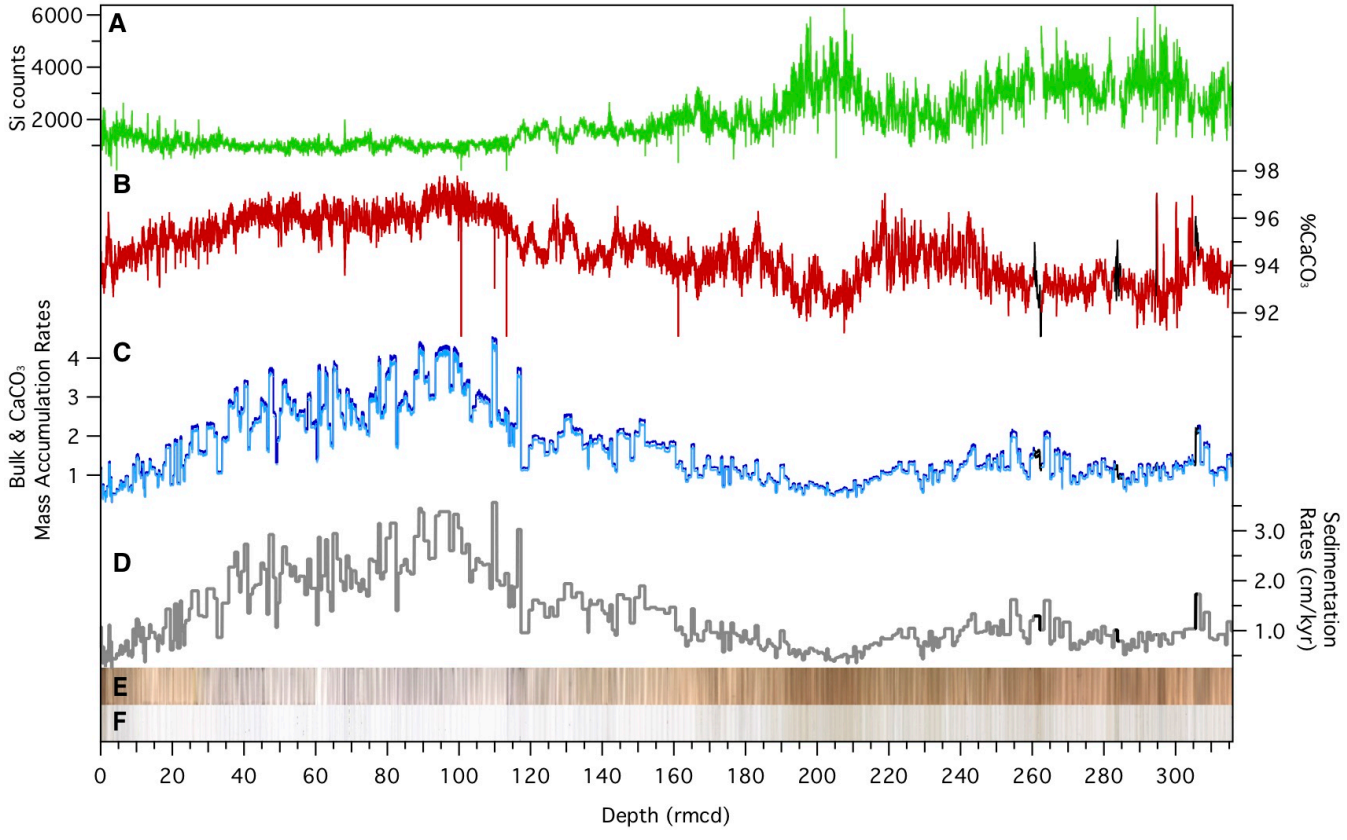

https://doi.org/10.5194/cp-2020-108
Preprint. Discussion started: 4 September 2020

Climate of the Past Discussions
Open Access
EGU

Figure 4: Wavelet spectra in the depth domain of (A) the XRF-derived %$CaCO_3$ data for Sites 1264 and 1265. The %$CaCO_3$ data has been detrended to remove all cycles (B) greater than 2 m or (C) greater than 40 m. The wavelets were generated using the code from Torrence and Compo (1998) and Grinsted et al. (2004).

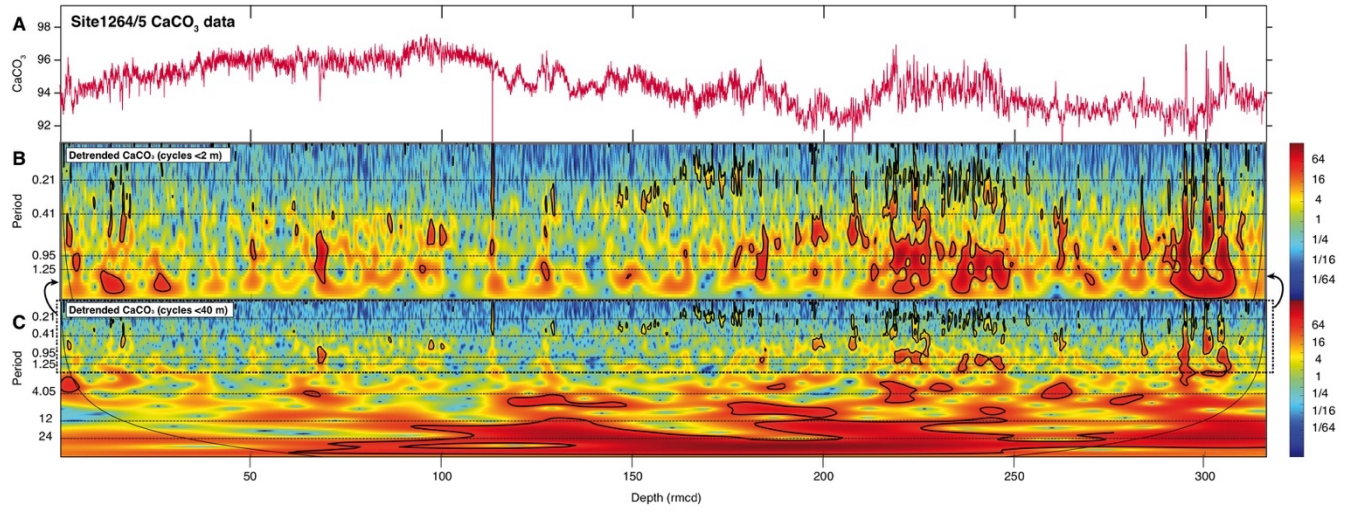

5

https://doi.org/10.5194/cp-2020-108
Preprint. Discussion started: 4 September 2020

Climate of the Past Discussions

Figure 5: Overview of the new astrochronology for the last 30 Myr. The four panels show the different tuning strategies employed. I.a) 30-9.7 Ma: $CaCO_3$(/benthic $\delta^{18}O$) to eccentricity; I.b) 9.7-8.0 Ma: $CaCO_3$ to E(T); II) 8.0-3.3 Ma: $CaCO_3$(/benthic $\delta^{18}O$) to ET-P; and III) 3.3-0.0 Ma: benthic $\delta^{18}O$ to LR04. The composite core photo compiled from line scan images is used here as it highlights the sedimentological cyclicity best.

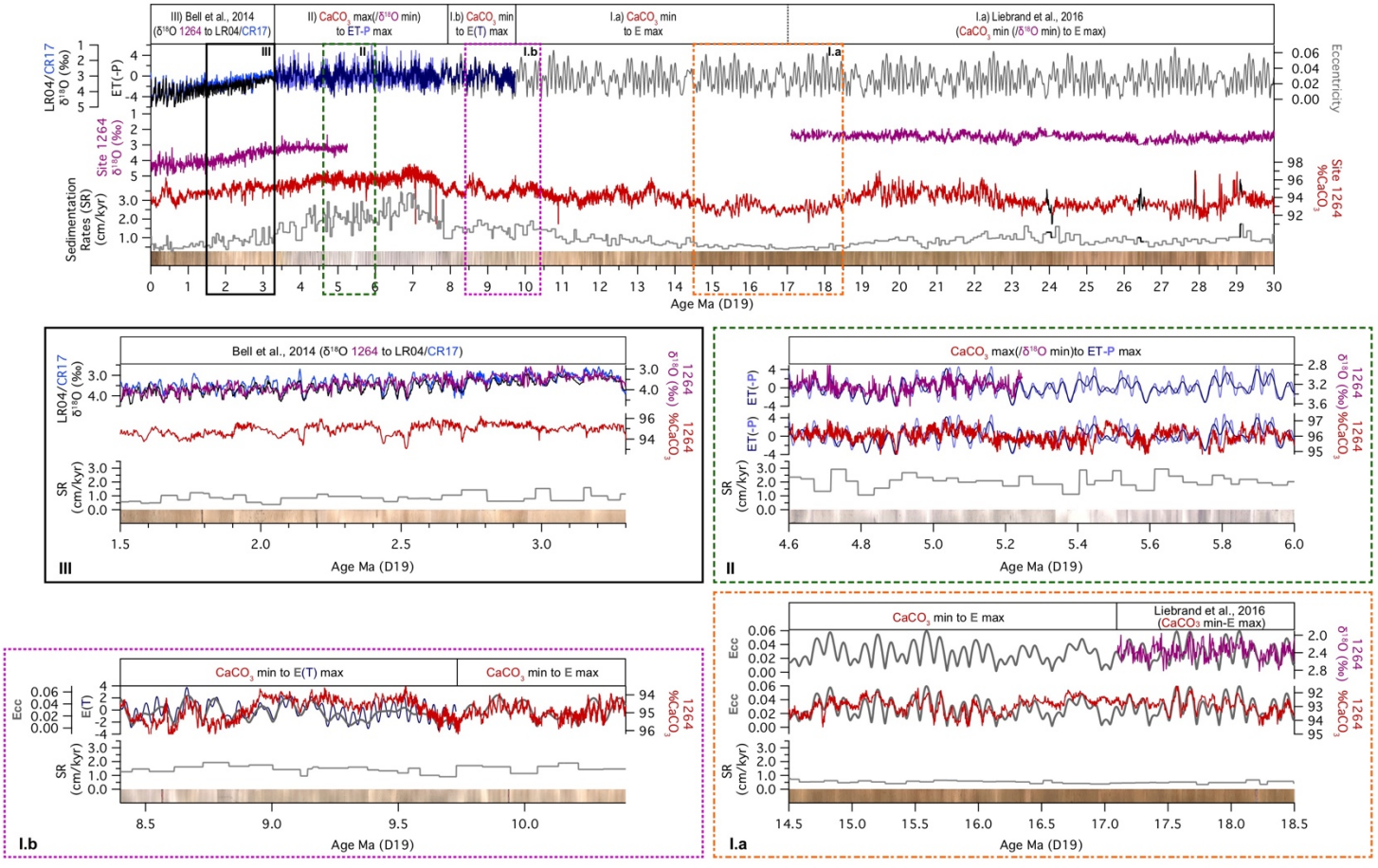

https://doi.org/10.5194/cp-2020-108
Preprint. Discussion started: 4 September 2020

Climate of the Past Discussions

Figure 6: New data from Sites 1264/1265 on the new astrochronology: A) Site 1264 benthic foraminiferal $\delta^{18}O$ (Bell et al., 2014; Liebrand et al., 2016) and the benthic $\delta^{18}O$ Megasplice (De Vleeschouwer et al., 2017); B) Site 1264 Si intensity (counts); C) left axis: %>63µm coarse fraction (%CF) (Keating-Bitonti and Peters, 2019) and right axis: XRF-derived $CaCO_3$ data from Sites 1264 (dark red) and 1265 (black); D) bulk and $CaCO_3$ MARs for Sites 1264 (dark and light blue, respectively) and 1265 (black and grey, respectively); E) Eccentricity and F) obliquity solutions (Laskar et al., 2004); G) line scan and H) core box photo Site 1264/1265 composite core photos; I) wavelet spectra in the time domain of the $CaCO_3$ data detrended to remove cycles over 200 kyr; J) wavelet spectra in the time domain of the $CaCO_3$ data detrended to remove cycles over 4 Myr (Torrence and Compo, 1998; Grinsted et al., 2004)..

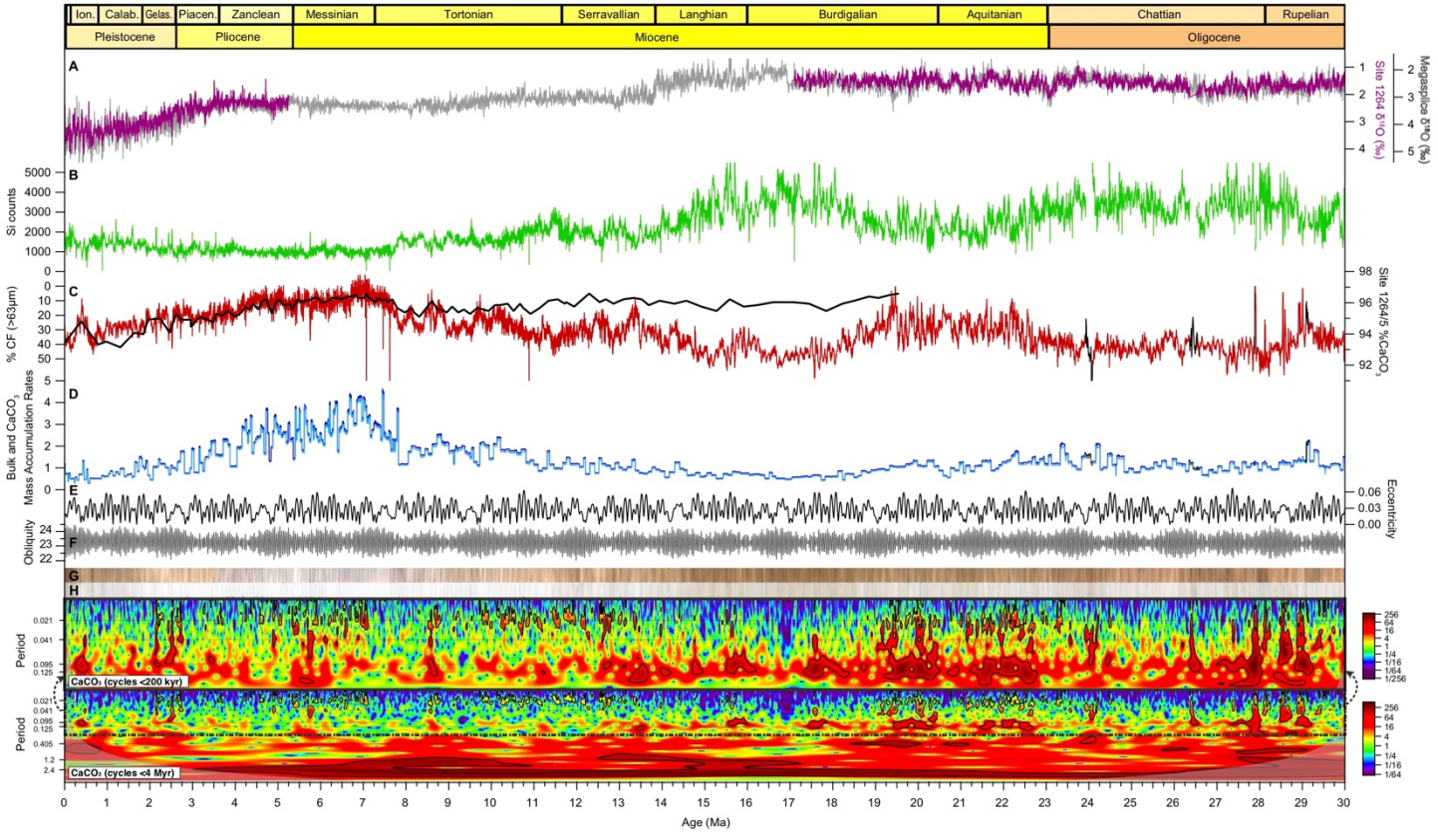

https://doi.org/10.5194/cp-2020-108
Preprint. Discussion started: 4 September 2020

Climate of the Past Discussions

Figure 7: Mid-late Miocene Sites 1264/1265 data on the new astrochronology: A) BAYSPAR TEX_{86} SSTs from Site 608 (blue dots = 50th percentile; medium blue = 65% CL; light blue = 95% CL; Super et al., 2018) B) benthic $\delta^{18}O$ Megasplice (De Vleeschouwer et al., 2017); C) XRF-derived $CaCO_3$ data from Site 1264; D) bulk and $CaCO_3$ MARs for Sites 1264 (dark and light blue, respectively); E) Site 1264 line scan and F) core box composite core photos; G) wavelet spectra in the time domain of the $CaCO_3$ data detrended to remove cycles >200 kyr (Torrence and Compo, 1998; Grinsted et al., 2004).

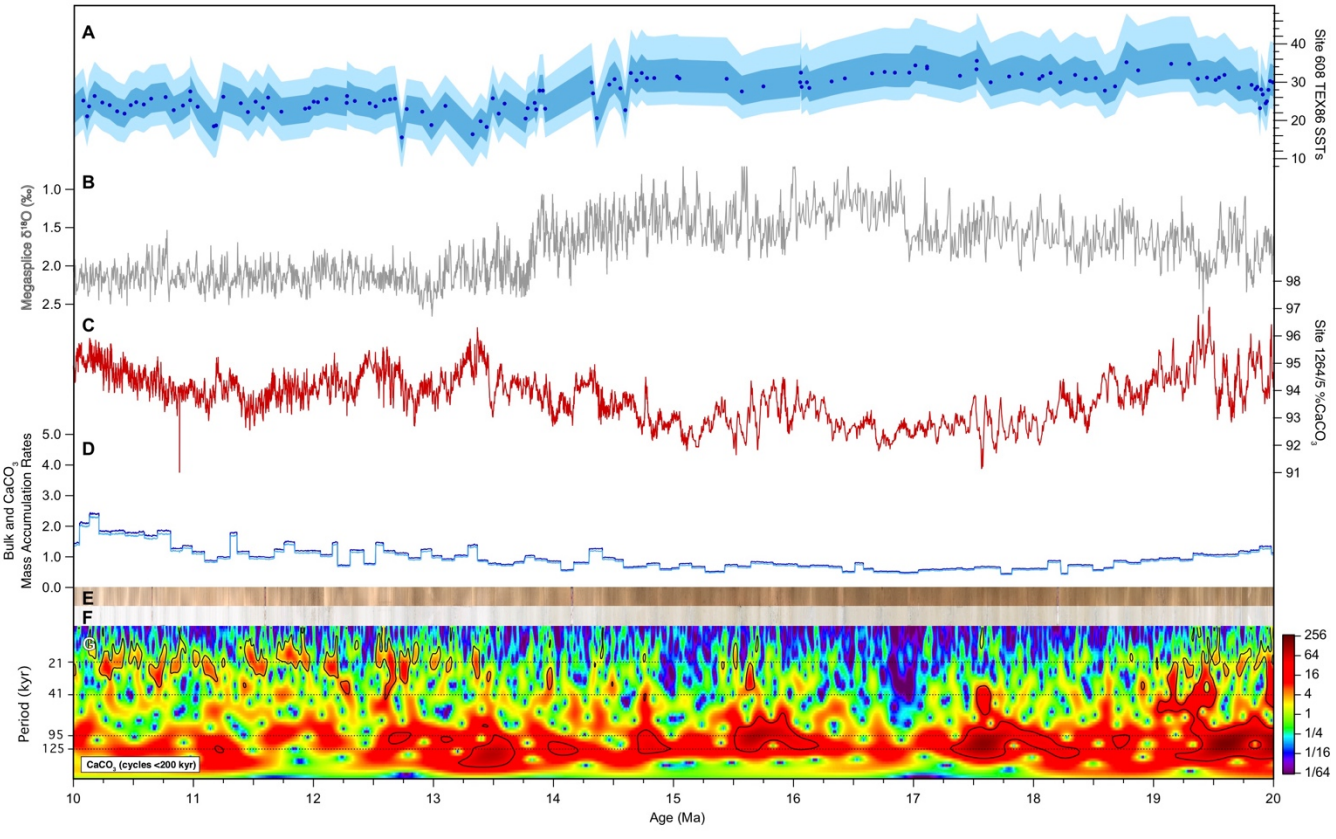

https://doi.org/10.5194/cp-2020-108
Preprint. Discussion started: 4 September 2020

Climate of the Past Discussions

Figure 8: Late Miocene to present data on the new astrochronology: A) left axis: XRF-derived $CaCO_3$ data from Sites 1264 (dark red) and right axis: >63µm coarse fraction (%CF) (Keating-Bitonti and Peters, 2019); B) normalised Site 1264 MARs (this study) and a normalised eastern equatorial Pacific (EEP) stack comprising data from ODP Sites 848, 849, 850 and 851, and IODP Sites U1335, U1337 and U1338; (Lyle et al., 2019); C) Site 1264 $CaCO_3$ MARs; D) MARS from EEP ODP Sites 848, 849, 850 and 851, and IODP Sites U1335 and U1338 (Lyle et al., 2019). Site U1337 was not included as it was partly affected by winnowing (see Lyle et al., 2019 for details).